

UNDER PRESSURE: BIOMECHANICS OF BUOYANCY IN BULL KELP

(*NEREOCYSTIS LUETKEANA*)

by

Lauran Liggan

BSc, Humboldt State University, Arcata, 2013

A THESIS SUBMITTED IN PARTIAL FULFILLMENT OF THE REQUIREMENTS

FOR THE DEGREE OF

MASTER OF SCIENCE

in

THE FACULTY OF GRADUATE AND POSTDOCTORAL STUDIES

(Botany)

THE UNIVERSITY OF BRITISH COLUMBIA

(Vancouver)

April 2016

© Lauran Liggan, 2016

Abstract

Maintaining buoyancy with pneumatocysts is essential for subtidal seaweeds with long flexible thalli, such as *Nereocystis luetkeana* (*Nereocystis*), to achieve an upright stature and compete for light. However, as *Nereocystis* grows, pneumatocysts are exposed to significant changes in hydrostatic pressure. Exposure to changing hydrostatic pressure could cause complications since the pneumatocyst is filled with gases that may expand or contract, potentially causing pneumatocysts to break, flood, and no longer be buoyant. This study explored how *Nereocystis* pneumatocysts resist biomechanical stress and keep the developing sporophyte upright in the water.

Throughout development, pneumatocysts had an internal pressure consistently less than atmospheric pressure (3 – 100 kPa), indicating pneumatocysts always experience compressional loads. The structural integrity and design of the pneumatocyst to resist buckling was assessed by measuring compressional modulus (material stiffness), calculating material stress, analyzing critical geometry, and estimating critical buckling pressure. Small pneumatocysts found at depth (inner radius = 0.8 - 0.9 cm; wall thickness = 0.2 cm) were demonstrated to have reached a critical size in development and are at greatest risk of buckling. Pneumatocysts do not adjust material properties or geometry to reduce wall stress, but they are naturally resistant to hydrostatic loads. Critically small pneumatocysts are estimated to buckle at 35 m depth, which was observed to be sporophytes' lower limit in the field. Data suggest that hydrostatic pressure, not just light limitation, might explain the maximum depth to which *Nereocystis* is capable of growing.

Pneumatocyst gas composition did not change throughout development, and contrary to previous studies, internal gas concentrations were different from the

atmosphere with O₂, N₂, CO, and CO₂ concentrations of 59%, 40%, 1.6%, and 0.6% respectively. Furthermore, pneumatocyst surface area to volume ratio did not correlate with the exchange of gases produced from photosynthesis and respiration. As sporophytes grow, total buoyant force is steadily outpaced by the weight of growing thalli, and the risk of the pneumatocyst sinking increases. Adult sporophytes are estimated to sink when pneumatocysts volume reaches 1.3 L, close to the maximum observed size in the field.

Preface

Chapter 1 and 2 are based on work conducted in the Martone Laboratory (Botany Department, University of British Columbia) and at the Bamfield Marine Sciences Centre on Vancouver Island. I was responsible for collecting all data reported in the lab and the field. Research was funded by an NSERC Discovery grant to Dr. Patrick Martone.

My research supervisors, Dr. Patrick Martone and Dr. Margo Lillie (Zoology Department), aided in data analyses and chapter revisions during the writing of the thesis. Dr. Christopher Harley (Zoology Department) also contributed to the final revisions of the thesis.

Table of contents

Abstract.....	ii
Preface.....	iv
Table of contents.....	v
List of tables	viii
List of figures	ix
Acknowledgements.....	xiii
Introduction	1
Chapter 1: Effects of hydrostatic pressure on pneumatocyst growth and development.....	5
1.1 Introduction	5
1.1.1 Ecology and life history	5
1.1.2 Understanding responses to hydrostatic pressure	6
1.1.3 Pneumatocyst material stress and the risk of breaking	9
1.1.4 Study objectives	10
1.2 Methods	11
1.2.1 Sample collection	11
1.2.2 Measuring internal pneumatocyst pressure.....	12
1.2.3 Calculating wall stress	15
1.2.4 Compressive modulus	16
1.2.5 Quantifying changes in pneumatocyst geometry	19
1.2.6 Calculating pneumatocyst environmental safety factor.....	20

1.3 Results	21
1.3.1 Changes in pneumatocyst volume and internal pressure	21
1.3.2 Calculated wall stress	26
1.3.3 Pneumatocyst wall material properties	27
1.3.4 Pneumatocyst geometry	27
1.3.5 Pneumatocyst safety factor	31
1.4 Discussion	32
1.4.1 Changes in pneumatocyst internal pressure and volume	32
1.4.2 Pneumatocyst wall stress and the risk of buckling	34
1.4.3 Reducing wall stress	35
1.4.4 Pneumatocysts at risk of buckling	36
1.4.5 At what depth will a small pneumatocyst break?	37
1.4.6 Conclusion	38
Chapter 2: Developmental changes in gas composition and buoyancy of	
<i>Nereocystis</i> pneumatocysts	40
2.1 Introduction	40
2.1.1 Growth and development	40
2.1.2 Pneumatocyst gas composition and production	41
2.1.3 Pneumatocyst buoyancy	43
2.1.4 Study objectives	43
2.2 Methods	44
2.2.1 Specimen collection	44
2.2.2 Internal gas composition	45

2.2.3 Pressure and CO ₂ fluctuations	47
2.2.4 Buoyant force	50
2.2.5 Buoyant safety factor	52
2.3 Results	53
2.3.1 Pneumatocyst gas composition	53
2.3.2 Pressure and CO ₂ fluctuations	57
2.3.3 Pneumatocyst buoyancy	59
2.4 Discussion	61
2.4.1 Pneumatocyst gas composition	61
2.4.2 Pressure and CO ₂ fluctuations	64
2.4.3 Pneumatocyst buoyancy	65
2.4.4 Conclusion	67
Conclusion	69
Future directions	72
References	76

List of tables

Table 1: Table showing calculated ESF values for 4 pneumatocysts collected between 2.7 m and 6 m..... 31

Table 2: Estimated critical breaking depth and breaking stress for 2 small pneumatocysts (with critical geometry) recorded to have the greatest wall stresses and the greatest r; t found between 7 and 8 m of seawater..... 31

Table 3: Table showing average gas concentrations of air and a pneumatocyst. Standard deviation of gas concentrations in a pneumatocyst is expressed in. Pneumatocyst gas concentrations were compared to atmospheric gas concentrations by using information available online from the National Oceanic and Atmospheric Administration (NOAA.gov, USA) 56

Table 4: Table showing buoyant factor (BSF) calculated from 5 large pneumatocysts. Average BSF is 2.18 ± 1.3 60

List of figures

Figure 1: Diagram of *Nereocystis luetkeana* sporophyte (Denny et al. 1997). Scale bar is 1 m (Denny et al. 1997)..... 3

Figure 2: Diagram of a pneumatocyst under pressure. Arrows indicate direction of force where pressure is applied. The force differential (ΔF) is expressed in the equation above where P_o = external hydrostatic pressure, r_o = the outer radius, P_i = internal pneumatocyst pressure, and r_i = the internal radius..... 7

Figure 3: Model of how a balloon would act to changes in hydrostatic pressure using eqn. 1.1. Expected changes in internal balloon pressure and depth decreases (A). Expected changes in balloon volume as depth decreases (B)..... 8

Figure 4: A) Location of Victoria (circled), British Columbia Canada on the southern end of Vancouver Island B) Map of Ogden Point Breakwater. White line represents area where whole thalli were collected between 0 and 9 meters of seawater (provided by Google Maps)..... 11

Figure 5: Diagram of water manometer. Pneumatocysts were punctured using a lubricated syringe needle. Gauge pressure was calculated by the equation above where ρ = density of water 1000 kgm^{-3} , $g= 9.81 \text{ ms}^{-2}$, h = height of water moved in both arms post puncture, and P_{ATM} = atmospheric pressure..... 14

Figure 6: Instron design for tension-compression tests. Top cross-beam is 9 cm width x 0.8 cm length and the base block is 8 cm width x 8 cm length. Pneumatocyst samples cut into doughnuts or cubes are glued to both the cross beam and the block. Black arrows indicate direction of tension and compression during data collection..... 17

Figure 7: Stress-Strain curves for one sample showing 4 cycles of compression and tension. The black bracket indicates where compressive modulus was measured (slope of the line) at 1% (0.01mm/mm) compression during the 2nd cyclic cycle..... 18

Figure 8: Pneumatocyst volume at various depths (A). Pneumatocyst internal pressure at various depths (B). Red dotted line indicates atmospheric pressure..... 22

Figure 9: Average internal pressure for small (8-20 cm³) pneumatocysts, found shallow (<2 m) and at depth (>8 m). Error bars indicate standard deviation of internal pressure (Shallow ± 16.86 kPa; Deep ± 16.82 kPa) for each pneumatocyst depth group ($t = 1.03$; $df=13.6$; $P>0.1$)..... 23

Figure 10: Internal pneumatocyst pressure and total pneumatocyst gas as a function of pneumatocyst volume..... 24

Figure 11: Blue data points: internal pneumatocyst pressure plotted with pneumatocyst depth (0-9m). Green data points: external hydrostatic pressure plotted with depth (0-9m)..... 25

Figure 12: Pneumatocyst wall stress at depths between (0-9m)..... 26

Figure 13: Young’s modulus for different pneumatocyst volumes..... 27

Figure 14: Estimated wall stress at depths from 0-9m for a given $r_i:t$ ratio (1:1,3:1,and 6:1; A). Dashed line indicates estimates of wall stress for a given $r_i:t$ ratio at 6 m. $r_i:t$ ratio at depths between 0-9m ($P>0.05$; B) 28

Figure 15: Pneumatocyst wall stresses for small pneumatocysts with different $r_i:t$ ratios. All pneumatocysts were collected between 7 and 8.7 m 29

Figure 16: Inner pneumatocyst radius at different depths (A). Grey data points are samples that began growing below 9 m and thus growth data is missing from the

substratum to 9 m. These data were not included in analyses of pneumatocyst development. Pneumatocyst wall stress with an inner pneumatocyst radius (B). Black dotted line indicates overall trend in wall stress as inner radius increases. $r_i:t$ ratio with inner radius from (C). Black circle indicates pneumatocysts with the greatest wall stresses shown in part B. Inner pneumatocyst radius with pneumatocyst tissue volume (D)..... 30

Figure 17: Map of southern Vancouver Island, British Columbia Canada. The yellow circle indicates location of Bamfield (A). Map of field sites where *Nereocystis* was collected (B) (provided by Google Maps)..... 45

Figure 18: Diagram of Q trak sensor. CO₂ and CO concentrations in the pneumatocyst were calculated using the equation above. Where C₁= the concentration read on the monitor (ppm), V₁= volume of the calibration wand (ml), C₂= unknown pneumatocyst concentration (ppm), and V₂= 0.5 ml sample..... 46

Figure 19: Diagram of water manometer. Pneumatocysts were punctured using a lubricated syringe needle. Gauge pressure was calculated by the equation above where ρ = density of water 1000 kgm⁻³, g = 9.81 ms⁻¹, h = height of water moved in both arms post puncture, and P_{ATM} = atmospheric pressure. 48

Figure 20: Diagram of contraption designed to measure net buoyant force of the intact thallus. Whole kelp is placed in basket and applies an upward force that is detected by a force transducer..... 51

Figure 21: Concentrations of CO, CO₂, O₂, and estimated N₂ for different pneumatocyst volumes (P>0.05). Dotted lines indicate average gas concentration..... 54

Figure 22: Log total gas for different pneumatocyst volumes (10-1000ml)..... 55

Figure 23: Average concentrations of gases in air compared to average concentrations of gases in a pneumatocyst. Pneumatocyst gas concentrations were compared to atmospheric gas concentrations by using information available online from the National Oceanic and Atmospheric Administration (NOAA.gov, USA)..... 56

Figure 24: Log inner surface area to volume ratio (SA:V) for various pneumatocyst volumes (A). The total change or fluctuation of CO₂ for experimental pneumatocysts of various pneumatocyst volumes (B). SA:V is estimated with the regression model in part A. Grey dotted line indicates the average fluctuation of CO₂..... 57

Figure 25: Changes of light (A), internal pneumatocyst pressure (B), and CO₂ concentration (C) during a 24 hour time period starting at 21:30. All data points represent average values. Error bars indicate standard deviation..... 58

Figure 26: Log thallus weight (downward force, N) as a function of pneumatocyst volume (A). Log net buoyancy (upward force measured in Fig 20, N) as a function of pneumatocyst volume (B). Log total buoyant force (upward force, N) as a function of pneumatocyst volume. Dotted line indicates average total buoyant force (C; P>0.05).... 59

Figure 27: Log buoyant safety factor (BSF) as a function of Log pneumatocyst volume. The last 5 data points are represented in table 4..... 60

Acknowledgements

This study would have not been successful without the help and support from a handful of people. I would first like to thank my supervisor Dr. Patrick Martone, for giving me the much needed guidance, patience, and support to begin and accomplish my first attempt conducting research and developing my own ideas. His enthusiasm for science, seaweeds, and the marine world inspired me to be passionate about my work. I would also like to thank Dr. Margo Lillie who advised and guided me through out this project. Margo imparted her knowledge and experience conducting research in the field of biomechanics, which helped me frame and design my thesis.

The Bamfield Marine Sciences Centre provided much needed lab space for the majority of this study. All equipment used for the transport of pneumatocyst gas samples were graciously donated from Dr. Andreas Christen in the Department of Geography and Atmospheric Science Program. Equipment for measuring CO₂ was donated by Dr. Santokh Singh and the Plant Physiology Lab.

My fieldwork was tedious and required a cohort of people to collect useful data in a timely manner. With out the SCUBA diving and snorkeling support of Kyra Janot, Sam Starko, Rachel Munger, Laura Borden, and Meagan Abele, this study would have been impossible. I am very grateful that the UBC Aqua Society provided me with endless training, SCUBA tanks, and other resources, which made these sub tidal collections possible. I would like to specially thank Sarah Calbick for being not only my field and lab assistant but also my confidant who helped me design better methods for collecting data and limiting bias. My lab mates are amazing and I am very thankful to have had the opportunity to befriend and learn from each of them. They spent precious time to read my manuscripts and listen to countless practice talks through out this study.

I would like to thank my parents, Susan and Stuart Liggan for financially supporting me throughout my educational career. They have been nothing but positive about my passion for marine science and I cannot thank them enough for exposing me to the marine world at a young age. With out them, my love for the sea would not exist.

And lastly, I would like to thank my partner and best friend Bartek Radziej. He kept me sane with just a smile and up beat attitude during my long absences conducting fieldwork, my late nights in the lab, and as I forced him to help me in the field. Without his unconditional support and kindness, I would have never been able to complete this degree.

Introduction

Photosynthetic organisms, such as trees and kelp, have evolved morphological characteristics that enable them to compete for light. Though these characteristics are diverse and cater to the particular ecosystem where each species thrives, they all serve the same purpose: maintain an upright posture while exposed to physical stresses. The ability to remain upright allows these organisms to increase light interception and, ultimately, increase photosynthesis to fuel growth and reproduction.

In terrestrial forests trees build unique three-dimensional ecosystems that house a diverse community of organisms (Brandt et al. 2014). Trees gain height and build complex environments by having rigid, reinforced trunks that allow them to grow upright against gravity (Woodward 2004). Trees augment their biomechanical properties by creating wood and adding girth through secondary growth (Fournier et al. 2006; Jung et al. 2016). The rigid and strong structure of trees allows them to tolerate environmental stress, resist toppling in storms, and support forest ecosystems (Sellier and Fourcaud 2009; Jung et al. 2016).

Similar to terrestrial forests, kelps build diverse three-dimensional forests in near-shore marine ecosystems (Arzee et al 1995). Kelps also grow tall (up to 45 m; Spalding and Foster 2003), but unlike trees, kelps generally do not develop thick trunks for structural reinforcement. Instead, some kelps produce slender, flexible thalli that are highly extensible and not very stiff, yet they still manage to remain upright (Koehl and Wainwright 1977). Kelps, such as the Giant Kelp (*Macrocystis pyrifera*) and the Bull Kelp (*Nereocystis luetkeana*), buoy their lax thalli toward the

surface by developing gas-filled floats (Stewart et al. 2007). Like trees, kelps are exposed to environmental stresses such as hydrodynamic forces, and the ability of kelp stipes to resist breakage has been well-studied (Denny et al. 2007). However, the ability of certain kelps to produce and maintain gas-filled floats underwater has been poorly studied (but see Dromgoole 1981) and deserves further examination.

Study system

Nereocystis luetkeana (K. Mertens) Postels et Ruprecht (*Nereocystis*) is a large ecosystem-forming kelp in the Order Laminariales. *Nereocystis* is typically found from depths up to 35 m and is geographically distributed in wave/current-exposed areas along the west coast of North America (Abbott and Hollenberg 1976; Spalding and Foster 2003). *Nereocystis* has an annual life history, appearing first as a young sporophyte in late winter, growing to adulthood by early summer, and reproducing and becoming senescent in autumn (Koehl and Wainwright 1977). Gametophytes, which are microscopic and filamentous, likely persist all year hidden in the rocky substratum (Springer et al. 2007). *Nereocystis* is capable of growing about 6 cm a day and can have a flexible thallus that is heavy and reaches massive sizes (Setchel 1947).

Like all kelps, the sporophyte morphology includes a holdfast, stipe, and blade. However, unlike other kelps that lie prostrate or grow upright by stiffening their stipes, *Nereocystis* has a bulbous gas-filled float, called a pneumatocyst, which is buoyant and keeps the flexible thallus upright in the water (Fig 1). As *Nereocystis* grows and becomes heavier, the pneumatocyst provides structural support for the thallus, exposing blades to

maximum light (Stewart et al. 2007). Without pneumatocysts, thalli could not remain upright, and would be left growing near the substrate, near hungry herbivores and in low light, ultimately decreasing fitness (Chenelot and Konar 2007). Therefore, *Nereocystis* must maintain a resilient pneumatocyst that can tolerate biological and physical stresses, such as the pressure gradient between internal gases and external hydrostatic pressure.

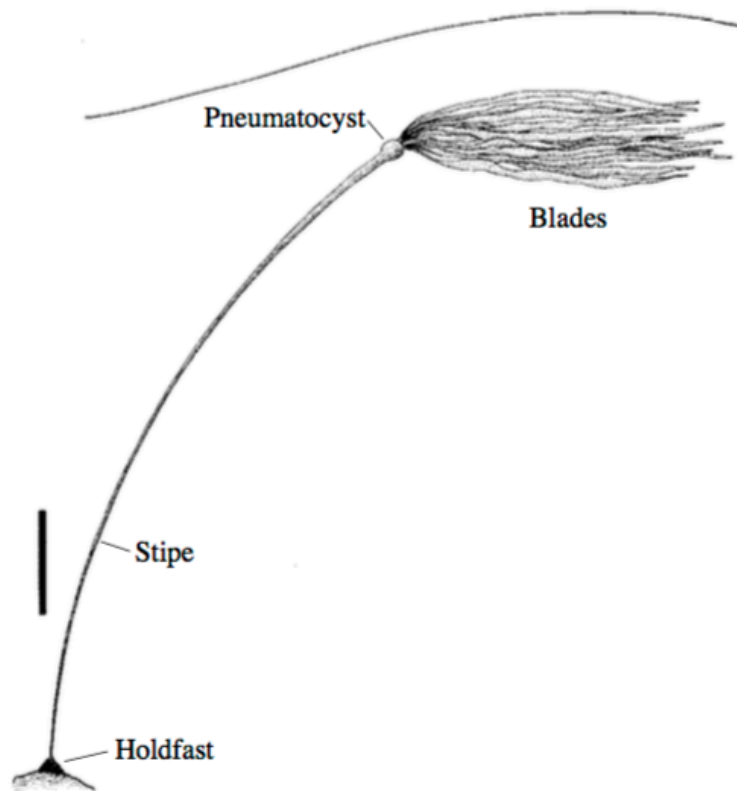


Figure 1: Diagram of *Nereocystis luetkeana* sporophyte (Denny et al. 1997). Scale bar is 1 m (Denny et al. 1997).

In Chapter 1, I investigate the structural design of *Nereocystis* pneumatocysts to resist buckling under hydrostatic loads. As sporophytes grow from 35 m depth, the developing pneumatocyst is exposed to changing hydrostatic pressure. This chapter explores how pneumatocysts change internal pressure and volume as they experience

different hydrostatic loads. Factors that would aid in reducing wall stress such as internal pressure, material properties, and geometry are measured to determine how pneumatocysts contend with applied loads and at what developmental stage they are at greatest risk of breaking. Furthermore, this study determines the maximum depth where pneumatocysts can develop.

In Chapter 2, I characterize the gas composition of pneumatocysts and determine if it changes as they grow and develop. I investigate whether physiological gases are added and subtracted to the pneumatocyst as a function of surface area to volume ratio, and predict which gases drive changes in internal pressure. Since the pneumatocysts are used to produce an upward buoyant force, this study determines how the buoyant force of the pneumatocyst changes to support the weight added to the fast growing sporophyte. In summary, this study gives a comprehensive overview of how the developing pneumatocyst of *Nereocystis* experiences and tolerates the dynamic physical environment.

Chapter 1

Effects of hydrostatic pressure on pneumatocyst growth and development

1.1 Introduction

1.1.1 Ecology and life history

Bull Kelp or *Nereocystis luetkeana* (*Nereocystis*) builds unique ecosystems in near-shore environments off the Pacific Northwest coast of North America. *Nereocystis* creates three-dimensional habitats by having a single gas-filled float called a pneumatocyst, which keeps the flexible thallus upright and vertical in the water column. *Nereocystis* as a primary producer has a large biomass that increases available nutrients which fuel not only marine, but also terrestrial ecosystems (Duggins and Simenstad 1989). Without this charismatic alga, the diversity of organisms in the subtidal world might otherwise be limited.

Nereocystis is an annual kelp, where fertilization, growth, and reproduction occur in one year. Young sporophytes are generally found no deeper than 30 to 35 m (Spalding and Foster 2003) and begin to grow rapidly toward the surface about 6cm a day (Scagel 1947). Like all kelp species, a young sporophyte begins its life as an upright with a simple holdfast, stipe and blade. Pneumatocysts begin to form within the transition zone between the stipe and the blade, about 2 weeks after germination (Nicholson 1970). During development, medullary cells along the transition zone begin to tear, releasing gas internally and creating the pneumatocyst (Dromgoole 1981). Once pneumatocysts have formed, sporophytes grow upwards and reach the surface in as little as 4 months (Duncan 1973). As thalli become larger, they increase biomass and become heavier, with blades

that can weigh up to 20 kg in air (Denny et al. 1997). The pneumatocyst increases volume as the thallus grows larger, extending into the stipe, increasing buoyancy to keep the heavy sporophyte upright. This upright posture helps the large flexible thallus increase light interception for the blades as the sporophyte grows from depth.

1.1.2 Understanding responses to hydrostatic pressure

Hydrostatic pressure exerted on a pneumatocyst is a compressive load that is applied along the outer surface of the structure. Since *Nereocystis* begins its life at depth and must grow up toward the surface, the pneumatocyst is exposed to changing hydrostatic pressure. Generally, pneumatocysts first develop when hydrostatic pressure is greatest and decreases over its lifetime. Being exposed to hydrostatic pressure could cause complications since the pneumatocyst is filled with gas, and if the pneumatocyst breaks, the thallus would flood and would no longer be buoyant. Pneumatocyst gas is incased in a thick wall (1-10 mm) where pressure created by these gases is exerted on the inner surface of the wall (Fig. 2). Hydrostatic pressure acts on the outer surface of the pneumatocyst wall creating a pressure gradient (Fig. 2). Since the pneumatocyst is a thick-walled structure, differences between the force applied on the outer wall by external pressure and the force applied on the inner wall by internal pressure (force differential) influences material stress. Stress generally is an internal distribution of forces within a material that balances and reacts to external loads applied. For a spherical object, like a young pneumatocyst, the inwards force due to hydrostatic pressure is acting over the outer surface area of the pneumatocyst wall and the internal pressure is acting over the inner surface area, creating material stress (Fig. 2). This force differential in the wall

conceivably puts the pneumatocyst at risk of breaking.

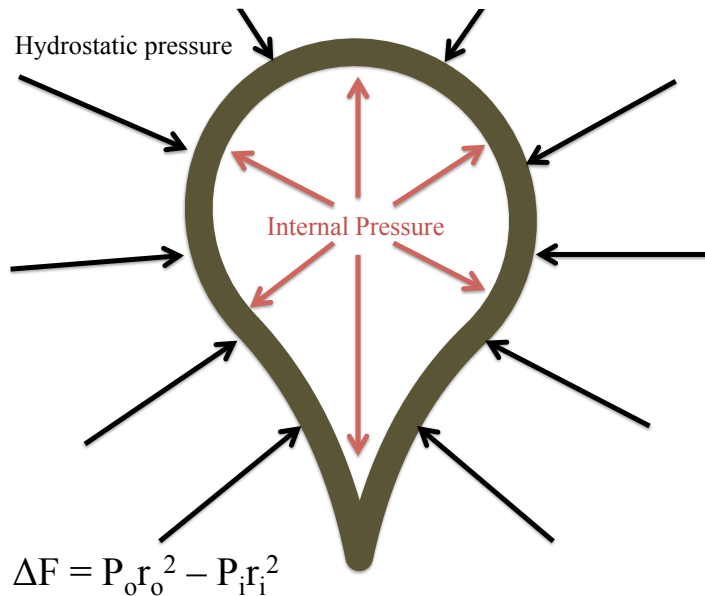


Figure 2: Diagram of a pneumatocyst under pressure. Arrows indicate direction of force where pressure is applied. The force differential (ΔF) is expressed in the equation above where P_o = external hydrostatic pressure, r_o = the outer radius, P_i = internal pneumatocyst pressure, and r_i = the internal radius.

Kelps that produce pneumatocysts for support prevent these structures from breaking under pressure by adjusting their structural and mechanical properties (Neushul and Haxo 1963). This suggests that investment, whether initial or continuous, is needed to ensure that the structural integrity of the pneumatocyst is not compromised when exposed to varying hydrostatic pressures. However, there is little knowledge of how these kelp grow and maintain the pneumatocysts' buoyant function despite varying hydrostatic pressure gradients.

Pneumatocyst development poses questions as to how hydrostatic pressure influences changes in volume and internal pressure. To understand how the forces on a pneumatocyst change as it grows from depth towards the surface, I begin by considering a very simple model: a thin-walled balloon, which is filled with air at a depth of 9 m, sealed, and then brought towards the surface. How changing hydrostatic pressure affects

the volume and internal pressure of this balloon can be calculated using Boyle's Law (eqn. 1):

$$P_1 V_1 = P_2 V_2 \quad (1)$$

where P_1 is the initial pressure and V_1 is the initial volume at 9 m, and P_2 and V_2 are the pressure and volume at any other depth. The temperature and number of moles of gas remain constant. In this example, I set P_1 at 192 kPa, which is hydrostatic pressure at 9 m, and V_1 at 1 cm³. I assume that the wall of the balloon is infinitely compliant so that the balloon passively responds to equilibrate internal pressure with the external hydrostatic pressure (Fig. 3A). As the balloon moves up through the water column from 9 m depth, hydrostatic pressure would decrease. Applying eqn. 1 shows how the balloon's volume would increase by a factor of 2 at the surface (Fig. 3B). If volume increases to the balloon's maximum capacity, then the balloon is at risk of tearing.

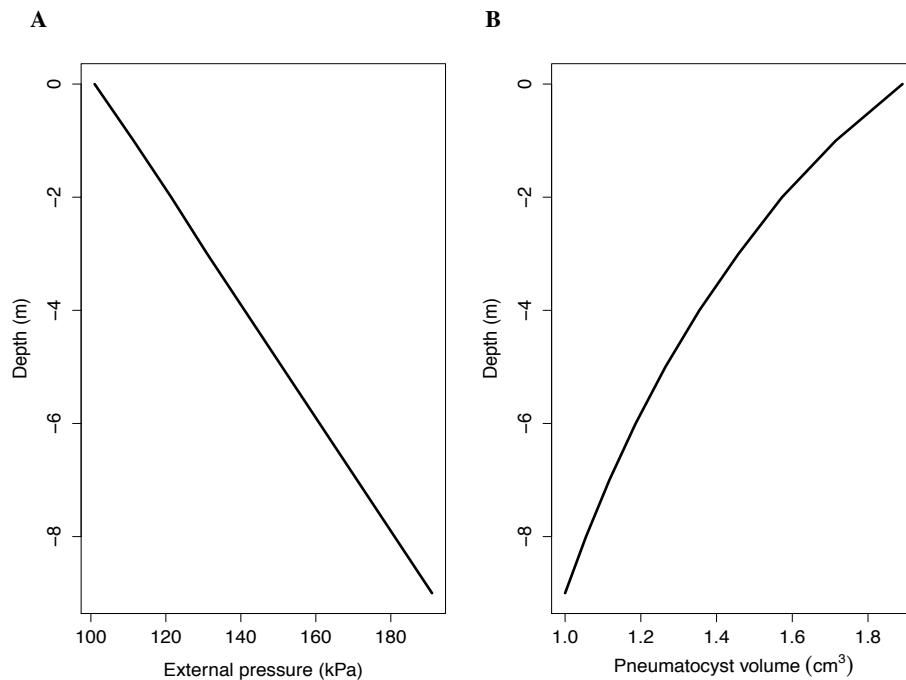


Figure 3: Model of how a balloon would act to changes in hydrostatic pressure using eqn. 1. Expected changes in internal balloon pressure and depth decreases (A). Expected changes in balloon volume as depth decreases (B).

1.1.3 Pneumatocyst material stress and the risk of breaking

As sporophytes grow from depth towards the surface, pneumatocysts experience different pressure gradients, ultimately causing stress on the pneumatocyst wall material. Unlike the balloon, the gas content is not constant in the pneumatocyst (see Ch.2) and the material properties of the wall are capable of withstanding material stresses, since they are found at depth. Since pneumatocysts found at depth are not smashed by hydrostatic pressure, the material is able to resist deformation and hinder changes in volume, preventing internal pressure from equilibrating with external pressure.

Theoretical analyses of optimally designed spherical capsules have yielded formulas to estimate critical breaking pressure (Huston and Josephs 2008). These formulas are generally estimates and disregard geometrical discontinuities and material imperfections (Huston and Josephs 2008). Regardless, these theoretical equations can be used to estimate the upper limits of critical breaking pressure or load. In this case, maximum hydrostatic pressure could be estimated for a spherical object such as a young pneumatocyst. Critical pressure is defined as the maximum force to break an object, and is a function of material stiffness (modulus), material deformity when loaded (Poisson's ratio: change in material volume when loaded), and the objects geometry/shape. For the case of a sphere, critical breaking pressure can be generalized using the following equation (Pan and Cui 2010; Pan et al 2010; Kármán and Tsien 1941):

$$P_{cr} = 0.37E / \left(\frac{t}{r}\right)^2 \quad (2)$$

Where P_{cr} is the critical breaking pressure, E is the modulus, 0.37 is a constant assuming a standard Poisson's ratio of 0.3 (changes in material volume when loaded) and deformation at the buckling point, t is the wall thickness, and r is the radius.

A pneumatocyst's geometry, material properties, and deformation due to the force differential (Fig. 2) directly influences the critical breaking pressure and thus the accumulation of material stress in the wall. To minimize wall stress, *Nereocystis* thalli could control the rate of hydrostatic pressure changes by adjusting the rate of stipe growth. However, stipe elongation is essential and allows the blades of *Nereocystis* to have maximum light availability. Therefore, pneumatocysts could adjust gas production to control internal pressure, maintaining a low force differential, or reduce wall stress by altering material properties such as modulus or geometry as they move through the water column.

1.1.4 Study objectives

In this study, I examine changes in volume and internal pressure as pneumatocysts develop from depth toward the surface. I investigate the extent to which pneumatocysts act like a passive balloon, changing volume and internal pressure as a function of the physical environment. I determine the pneumatocyst's pressure gradient and evaluate the forces it experiences. I also estimate at what point in the life of a sporophyte is pneumatocyst material stress greatest and, at this stage, I evaluate if pneumatocyst geometry, material properties, or the force differential help reduce overall wall stress, minimizing the risk of breaking. Finally, I determine if pneumatocysts are capable of tolerating high hydrostatic loads, which would determine if pneumatocysts are ever at risk of breaking at any given stage of sporophyte development.

1.2 Methods

1.2.1 Sample collection

Nereocystis thalli of varying volumes from 3 to 1200 cm³ were collected at Ogden Point Breakwater (Coordinates: 48.413542, -123.387235) in Victoria, British Columbia, Canada (n=72) (Fig. 4). Whole plants were haphazardly sampled with SCUBA from depths up to 9 m (Fig. 4).



Figure 4: A) Location of Victoria (circled), British Columbia Canada on the southern end of Vancouver Island B) Map of Ogden Point Breakwater. White line represents area where whole thalli were collected between 0 and 9 meters of seawater (provided by Google Maps).

All samples were detached from the substratum at the holdfast so that the pneumatocyst was fully intact. Collection depth of the holdfast, day, tidal height (at 0 m chart datum), and time were recorded for each sample. This was used to calculate the depth of a pneumatocyst based on the 0 m tide line (eqn. 3).

$$\text{Collected depth (m)} - \text{Tidal height (m)} = \text{Depth of Holdfast (m)} \quad (3)$$

$$\text{Depth of Holdfast (m)} + \text{Length of Stipe (m)} = \text{Depth of pneumatocyst at a 0 m tide}$$

External hydrostatic pressure (P_o) was estimated from pneumatocyst depth using eqn. 4:

$$P_o = (\rho gh) + P_{atm} \quad (4)$$

where P_o = calculated external hydrostatic pressure, ρ is the density of seawater (1025 kgm^{-3}), g is acceleration due to gravity (9.81 ms^{-2}), h is pneumatocyst depth, and P_{atm} is atmospheric pressure.

Pneumatocyst volume was recorded by carving a hole in the pneumatocyst, filling the inside with water and pouring it into a graduated cylinder. An average of 3 measurements was used to determine volume. Pneumatocyst length and width was measured using Image J 64 version 1.49 (National Institutes of Health) by taking photos of each sample with a meter stick. All statistical analyses were conducted using R version 0.99.467 (R Core Development Team).

1.2.2 Measuring internal pneumatocyst pressure

Water manometers (diameter: 4-8 mm; length: 20-60 cm) (Fig. 5) were used to measure internal pressure of the pneumatocysts directly after collection ($n=64$). Water manometers were attached to pneumatocysts using plastic tubing, a syringe, and a 21 gauge (0.7 mm) needle that was used to puncture pneumatocysts and measure the gas pressure inside (Fig. 5). All needles were lubricated with Vaseline to avoid air leaking during the manometer reading. Initial pressure readings were recorded no more than 30 seconds after the pneumatocysts were punctured. Internal pneumatocyst pressure was then calculated by using the dimensions of the manometer and the Ideal Gas Law with eqn. 5:

$$P_{gauge} V_{total} = nRT \quad (\text{Ideal Gas Law})$$

$$\begin{aligned}
&= (n_{Pn} + n_{mi})RT \\
&= \left(\frac{P_{Pn}V_{Pn}}{RT} + \frac{P_{mi}V_{mi}}{RT} \right) RT \\
&= P_{Pn}V_{Pn} + P_{mi}V_{mi} \\
P_{Pn} &= \frac{P_{gauge}V_{total} - P_{mi}V_{mi}}{V_{Pn}} \tag{5}
\end{aligned}$$

$$\text{Where } V_{total} = V_{Pn} + V_{mf}$$

where P_{Pn} is the unknown pneumatocyst pressure, P_{gauge} is the pressure reading from the manometer, V_{mf} is the total volume of the manometer from the water line to the needle after the pneumatocyst was punctured, P_{mi} is the pressure of the ambient air in the manometer, V_{mi} is volume of the manometer arm before the pneumatocyst is punctured and V_{Pn} is the volume of the pneumatocyst.

The ability to accurately measure internal pressure depended on differences in volume between the manometer arms and pneumatocysts: When pneumatocyst volume was significantly less than the manometer arm, the water level in the manometer arm barely moved, introducing error. The resolution of all manometer readings was 1 mm. Therefore, manometer error was estimated by adding and subtracting 1 mm from each measurement of water height (h), and then propagating this measurement error through the equation shown in Fig. 5 to estimate variation in P_{gauge} and pneumatocyst pressure (P_{Pn}) in eqn. 5. Larger differences between manometer arm and pneumatocyst volume yielded greater propagated error. Error bars therefore represent the maximum and minimum pressure for each recorded pneumatocyst pressure.

Measuring internal pressure at the surface could generate error if the pneumatocysts expand and change volume as they are brought from depth. Pneumatocyst

diameter was measured using calipers for each sample at depth and at the surface. There was a minimal change in diameter by 0.5 to 1 mm, which was mostly due to error using calipers while diving and handling other equipment underwater. Therefore, I assumed that pneumatocyst volume did not change enough to make pressure measurements at the surface inaccurate.

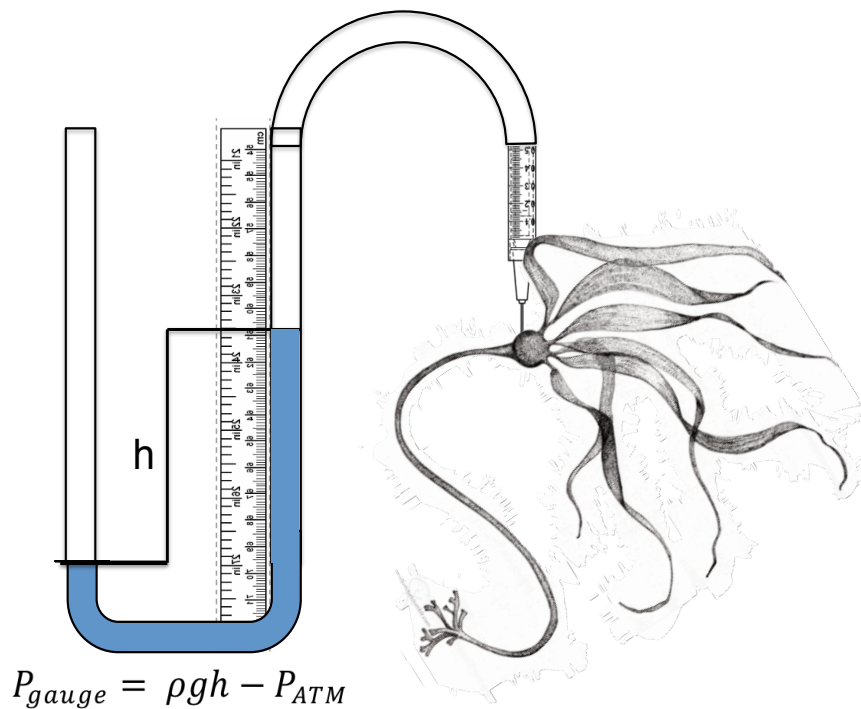


Figure 5: Diagram of water manometer. Pneumatocysts were punctured using a lubricated syringe needle. Gauge pressure was calculated by the equation above where ρ = density of water 1025 kgm^{-3} , $g = 9.81 \text{ ms}^{-2}$, h = height of water moved in both arms post puncture, and P_{ATM} = atmospheric pressure.

The confounding effects of pneumatocyst depth and volume could both affect internal pressure. Thus, by keeping pneumatocyst volume constant, I determined if internal pressure varied with depth. Pressure differences between small pneumatocysts found at depth and small pneumatocysts found near the surface ($n=28$) were tested using a t -test. All calculated pneumatocyst pressures were also plotted against pneumatocyst

depth and analyzed using linear regression analyses.

Internal pneumatocyst pressure was plotted against pneumatocyst volume and tested with a linear regression. Total molar concentration of pneumatocyst gases were plotted against pneumatocyst volume. Internal pneumatocyst pressure and external hydrostatic pressure were plotted against pneumatocyst depth to determine if the pneumatocyst's pressure differential (ΔP) changed with depth.

1.2.3 Calculating wall stress

Older pneumatocysts have two different geometries: a cylindrical hollow stipe and a spherical end. As mentioned previously, stresses are influenced by geometry and thus the cylinder portion of the pneumatocyst would experience a different magnitude of material stresses than the spherical end. A preliminary study was conducted to determine which portion of the pneumatocyst broke first. This was done by dropping 5 weighted thalli down to 50 m of seawater until they buckled, and revealed that the spherical end of pneumatocysts were at greatest risk of buckling. Thus, this study only focused on the average pneumatocyst wall stress accumulated in the spherical region of the pneumatocyst (eqn. 6). Eqn. 6 takes into consideration that the pneumatocyst is a thick-walled structure and therefore the outer portion of pneumatocyst wall experiences different loads than the inner portion of the pneumatocyst wall.

Average wall stress in a pneumatocyst at a specific depth was calculated using eqn. 6:

$$\sigma_{Avg} = \frac{P_o r_o^2 - P_i r_i^2}{r_o^2 - r_i^2} \quad (6)$$

Where σ_{avg} is the average circumferential stress in the pneumatocyst wall, P_o is the

external hydrostatic pressure applied to the outer surface of the pneumatocyst wall, P_i is the internal pneumatocyst pressure applied to the inner surface of the pneumatocyst wall, r_i is the internal pneumatocyst radius, and r_o is the outer pneumatocyst radius. Positive values indicated compressive stresses. All radii and wall thicknesses were measured using calipers to the nearest 1 mm. A linear regression analysis was conducted to determine if material stress changed with pneumatocyst depth.

1.2.4 Compressive modulus

Material properties of pneumatocyst walls were tested at the University of British Columbia in Vancouver, British Columbia Canada. Samples (n=33) were analyzed using an Instron 5500R (Model # 1122, Instron Inc. MA, USA). Pneumatocysts were cut into circular doughnuts or cubes to measure the elastic modulus of the material. Modulus is a material property and independent of volume or shape. The Instron was equipped with an 8 X 8cm block at the base and a 9 X 0.8 cm cross beam atop (Fig. 6). Samples were glued onto the top cross beam and the base block using super glue (Fig. 6). The integrity of the adhesion during a test was verified with a high-speed camera (Casio exilim. EX-FH25). Each sample was sprayed and hydrated with salt water before each test. Stress was measured by dividing force applied to the sample by its cross-sectional area. The movement (up or down) of the Instron crossbeam was used to measure strain. The modulus was calculated by dividing material stress with material strain (mm/mm) (i.e. slope of the Stress-Strain curve). Modulus was measured by putting each sample in compression and tension for 4 cycles. Based on preliminary tests (see below) compressional modulus was measured and recorded via the 2nd cycle at 1% compression

(Fig. 6; Fig. 7). A linear regression analysis was conducted to determine if modulus changed with pneumatocyst volume.

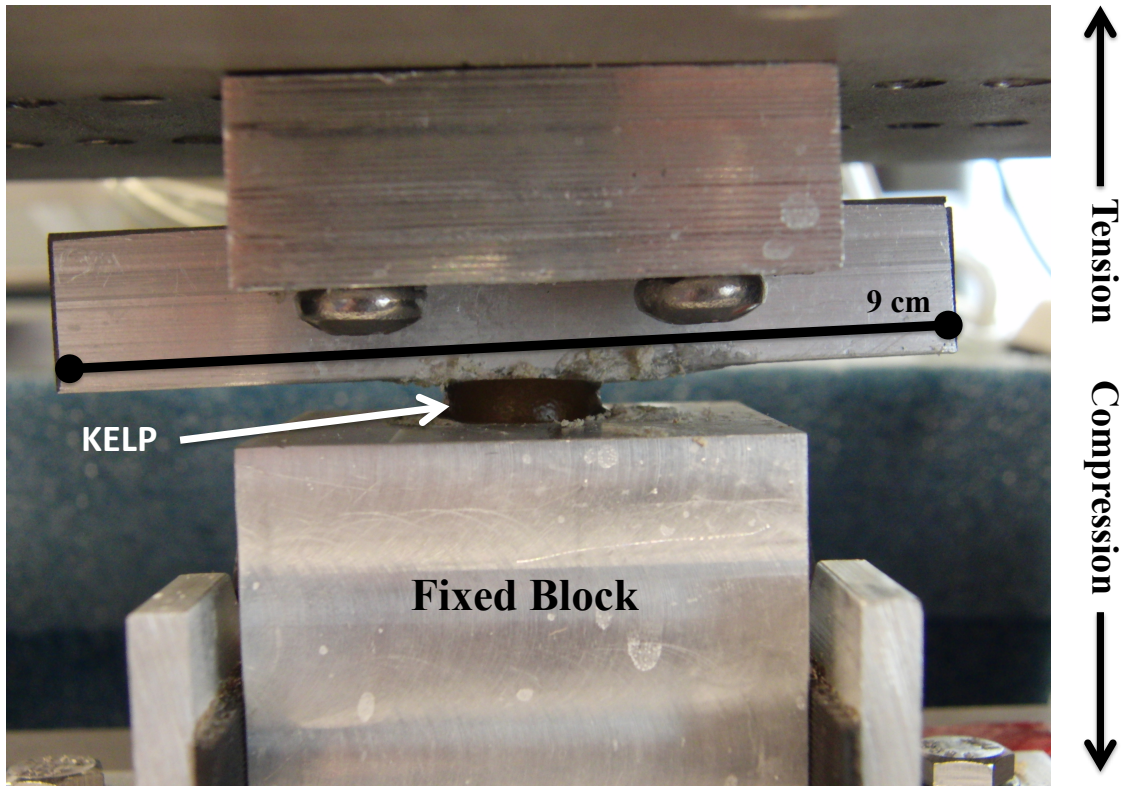


Figure 6: Instron design for tension-compression tests. Top crossbeam is 9 cm width x 0.8 cm length and the base block is 8 cm width x 8 cm length. Pneumatocyst samples cut into doughnuts or cubes are glued to both the cross beam and the block. Black arrows indicate direction of tension and compression during data collection.

Three preliminary tests were conducted to establish a suitable test protocol. Initially, all samples were subjected to tension and compression through 4 cycles (n=12). The modulus was higher for the first cycle (Mullin's Effect), but was constant for the 2nd, 3rd, and 4th cycle. Therefore, the 2nd cycle was used to measure modulus of pneumatocyst material.

Doughnut-shaped samples were exposed to 1, 3, 5, and 8% extension and compression (n=12). Compressive slopes were measured for each extension/compression series to determine if any of the extensions damaged the samples. All moduli appeared to be similar for every extension/compression and therefore the 1% extension method was used to measure modulus for all samples (Fig. 7).

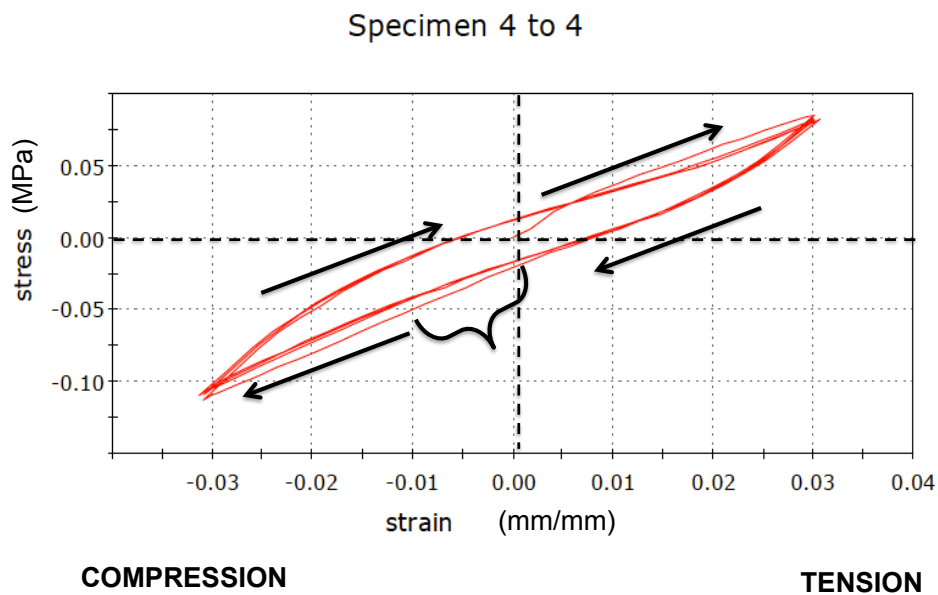


Figure 7: Stress-Strain curves for one sample showing 4 cycles of compression and tension. The black bracket indicates where compressive modulus was measured (slope of the line) at 1% (0.01 mm/mm) compression during the 2nd cyclic cycle.

Modulus measurements were tested for pneumatocyst samples cut into doughnuts and cubes with heights from 14 mm to 5 mm and widths from 14 mm to 5 mm (n=5). This determined if there was a size limitation to accurately measure samples glued in the Instron. Modulus measurement accuracy decreased once the sample was less than 8X8 mm. Therefore, all samples were cut to have a height (if doughnut) and width (if cubed) length no less than 8 mm.

1.2.5 Quantifying changes in pneumatocyst geometry

Measured pneumatocyst inner radius (r_i) and wall thickness (t) was used to determine the inner radius to wall thickness ratio ($r_i:t$). Changes in average material stress with increased depth (up to 9 m) were estimated for $r_i:t$ ratios from 1:1 to 6:1 using eqn. 6. The optimal $r_i:t$ ratio was determined by examining differences in average wall stress, arbitrarily at 5 m for the 1:1, 3:1, and 6:1 estimated ratio. These three ratios represented the total range of $r_i:t$ a pneumatocyst would have. Calculated $r_i:t$ ratios of all experimental pneumatocysts ($n=32$) were plotted against pneumatocyst depth and tested with linear regression analyses. A linear regression was also performed on $r_i:t$ ratios and average wall stress of small pneumatocysts ($n=12$) found at depths between 7 and 8.7 m. These data helped to determine the specific $r_i:t$ of a small deep pneumatocyst with the greatest calculated wall stress. Pneumatocyst inner radius ($n=72$) was plotted against depth. Average pneumatocyst wall stress was plotted against pneumatocyst inner radius (cm). The pneumatocyst $r_i:t$ ratio was plotted with pneumatocyst wall thickness ($n=64$). Pneumatocyst inner radius was lastly plotted with pneumatocyst tissue volume. Pneumatocyst tissue volume was calculated by estimating the total pneumatocyst volume (tissue and gas space) of a sphere from the pneumatocyst's measured outer radius (r_o) minus the pneumatocyst gas space spherical volume from the pneumatocyst's measured inner radius (r_i). These plots were made to demonstrate how pneumatocyst size, geometry, and tissue volume changed as they developed and grew larger.

1.2.6 Calculating pneumatocyst environmental safety factor

Four whole thalli were collected and average wall stress was estimated using eqn. 6. Each thallus was then placed into a weighted basket with a SCUBA analogue depth gauge (Scubapro MODEL # 28.019.900) and dropped down to 50 m. A video camera (Go-Pro Hero 3+ silver edition) recorded the sound and depth (in ft.) when each pneumatocyst buckled, detected by an audible “pop.” This depth was converted to hydrostatic pressure (eqn. 4) and then average breaking stress was calculated using eqn. 6.

The structural integrity of a pneumatocyst was assessed by calculating the pneumatocyst’s environmental safety factor (ESF). Generally, ESF is the ratio between the maximum load an object can withstand before breaking and the load it experiences day to day. Thus, by definition, ESF describes the difference between a structure’s design and its working stress. A structure can only support its maximum design load and no more. Any additional load will cause the structure to fail. For example, an ESF value of 1 indicates that a structure is just capable of tolerating loads it experiences day to day. As the ESF becomes larger that structural integrity of an object also becomes greater. The ESF of pneumatocysts were estimated by using eqn. 7.

$$ESF = \frac{\sigma_{break}}{\sigma_0} \quad (7)$$

Where σ_{break} is breaking stress of pneumatocyst wall and σ_0 is wall stress of pneumatocyst located at depths between 2 m and 6 m.

An average of the 4 previous ESF estimates were used to determine at what depth 2 collected small, young pneumatocysts ($r_i=0.8$ cm and 0.9 cm, $t=0.2$ cm) would break.

The estimated average ESF (3.9) was used to determine the pneumatocyst's breaking stress with eqn. 7. σ_{break} was then used in eqn. 6 to estimate the hydrostatic pressure where the pneumatocyst would break. These values were compared to theoretical projections using eqn. 2, assuming the modulus was 3.9 MPa. Modulus was determined by estimating modulus of small pneumatocysts with the regression line in Fig. 13.

1.3 Results

1.3.1 Changes in pneumatocyst volume and internal pressure

Pneumatocyst volume increased from 3 cm³ to 1200 cm³ as they grew from 9 m depth towards the surface (Fig. 8A). Small pneumatocysts between 3 cm³ and 50 cm³ were found at every depth and large pneumatocysts between 200 cm³ and 1200 cm³ were only found near the surface, above 2 m (Fig. 8A).

Internal pneumatocyst pressure did not significantly change with depth (Fig. 8B; $P > 0.05$). All internal pressures were less than atmospheric pressure (101 kPa), ranging from 3 to 100 kPa (Fig. 8B). Error bars indicate standard error of the manometer reading for a given sample. Manometer reading error was generally greatest when pneumatocysts were small or collected from great depth (Fig. 8B).

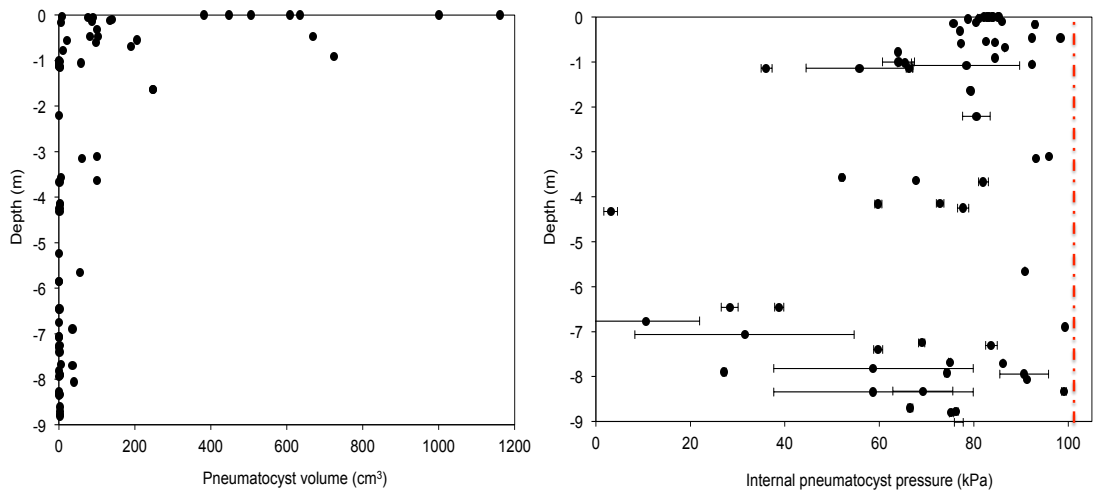


Figure 8: Pneumatocyst volume at various depths (A). Pneumatocyst internal pressure at various depths. Red dotted line indicates atmospheric pressure ($P>0.05$; B).

The confounding effects of pneumatocyst depth and volume could both affect internal pressure. However, there was no significant difference between the mean pressure values of small ($8\text{-}20\text{ cm}^3$) pneumatocysts found both at depth ($>8\text{ m}$) or near the surface ($<2\text{ m}$) (Fig. 9; t -test: $P>0.1$). The mean internal pressure for small pneumatocysts at the surface was $75\pm 17\text{ kPa}$ and the mean internal pressure for small pneumatocysts at depth was $61\pm 17\text{ kPa}$ (Fig. 9).

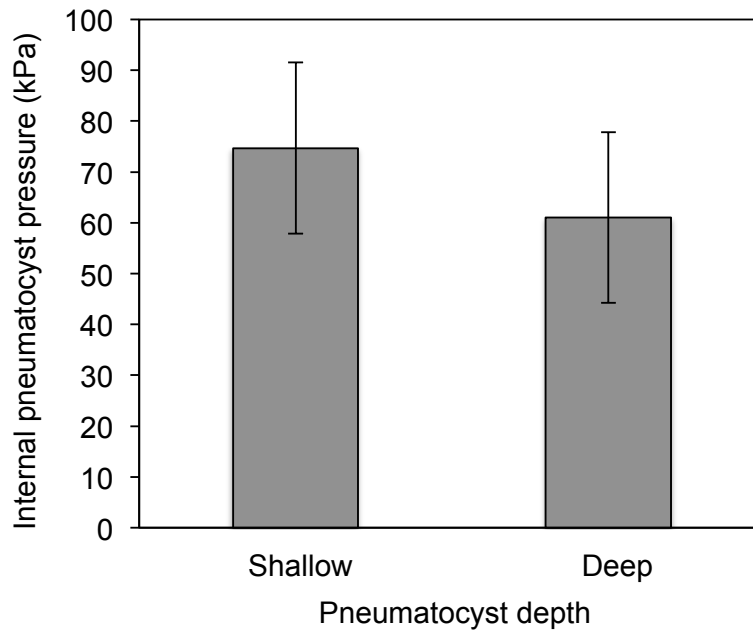


Figure 9: Average internal pressure for small (8-20 cm³) pneumatocysts, found shallow (<2 m) and at depth (>8 m). Error bars indicate standard deviation of internal pressure (Shallow ± 16.86 kPa; Deep ± 16.82 kPa) for each pneumatocyst depth group ($t = 1.03$; $df=13.6$; $P>0.1$).

As pneumatocyst volume increased from a minimum of 3cm³ to a maximum of 1200 cm³, pneumatocyst gas increased from 1.5X10⁻⁶ mol cm⁻³ to 4.25X10⁻⁵ mol cm⁻³ (Fig. 10), and pneumatocyst pressure increased from a minimum of 3 kPa, reaching an asymptote around 80 kPa (Fig. 10). Pneumatocysts greater than 200 cm³ had an internal pressure of 84±7 kPa (Fig. 10). Small pneumatocysts between 3 and 50 cm³ had variable internal pressures from 3 kPa to 100 kPa (Fig. 10). 6 of the small pneumatocysts found between 4 and 9 meters (Figs. 8A-8B) had the lowest internal pressures ranging from 3 to 40 kPa (Fig. 10).

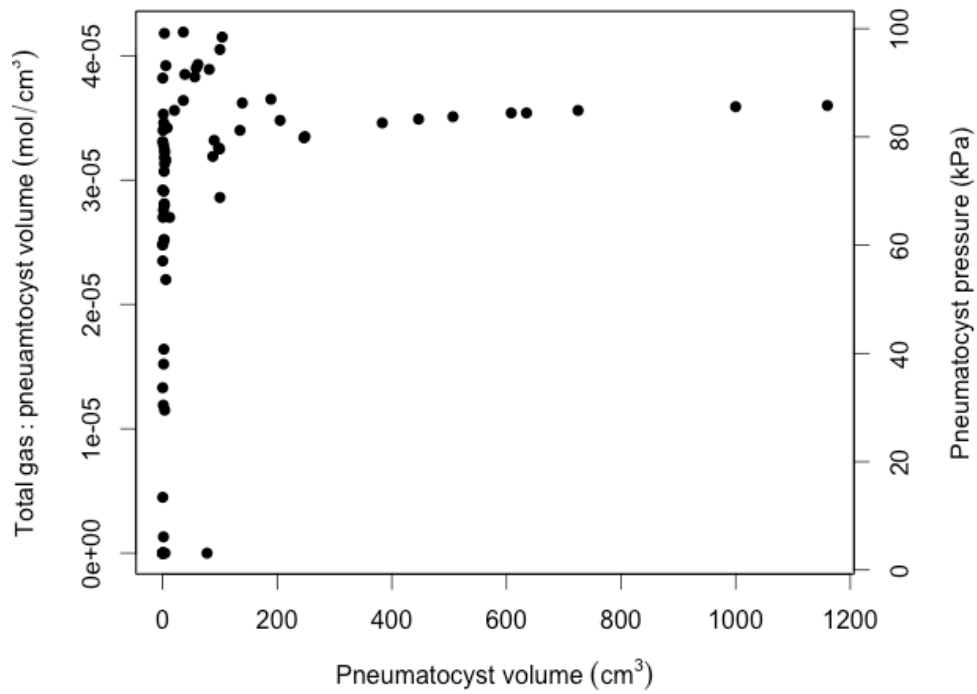


Figure 10: Internal pneumatocyst pressure and total pneumatocyst gas as a function of pneumatocyst volume.

Pneumatocyst internal pressure is less than external hydrostatic pressure at all depths (Fig. 11). Internal pneumatocyst pressure was generally 100 to 200 kPa less than external hydrostatic pressure below 4 meters (Fig. 11), and 1 to 50 kPa less above 3 m (Fig. 11).

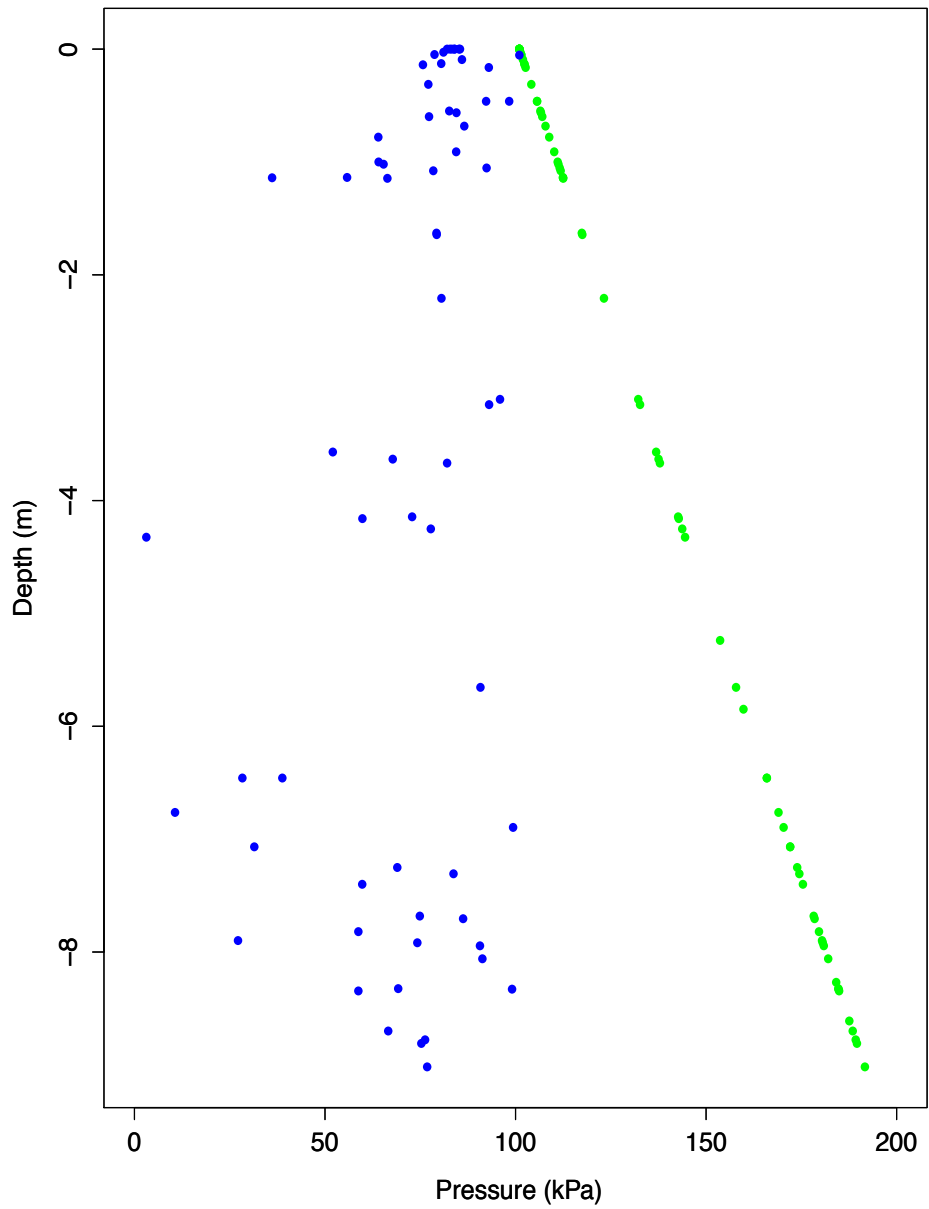


Figure 11: Blue data points: internal pneumatocyst pressure plotted with pneumatocyst depth (0-9m). Green data points: external hydrostatic pressure plotted with depth (0-9 m).

1.3.2 Calculated wall stress

Pneumatocyst wall stress significantly increased with depth (Fig. 12; $P < 0.001$, $R^2 = 0.69$). Pneumatocyst wall stress was maximum 460 kPa at 9 m depth and minimum 102 kPa at the surface (Fig. 12).

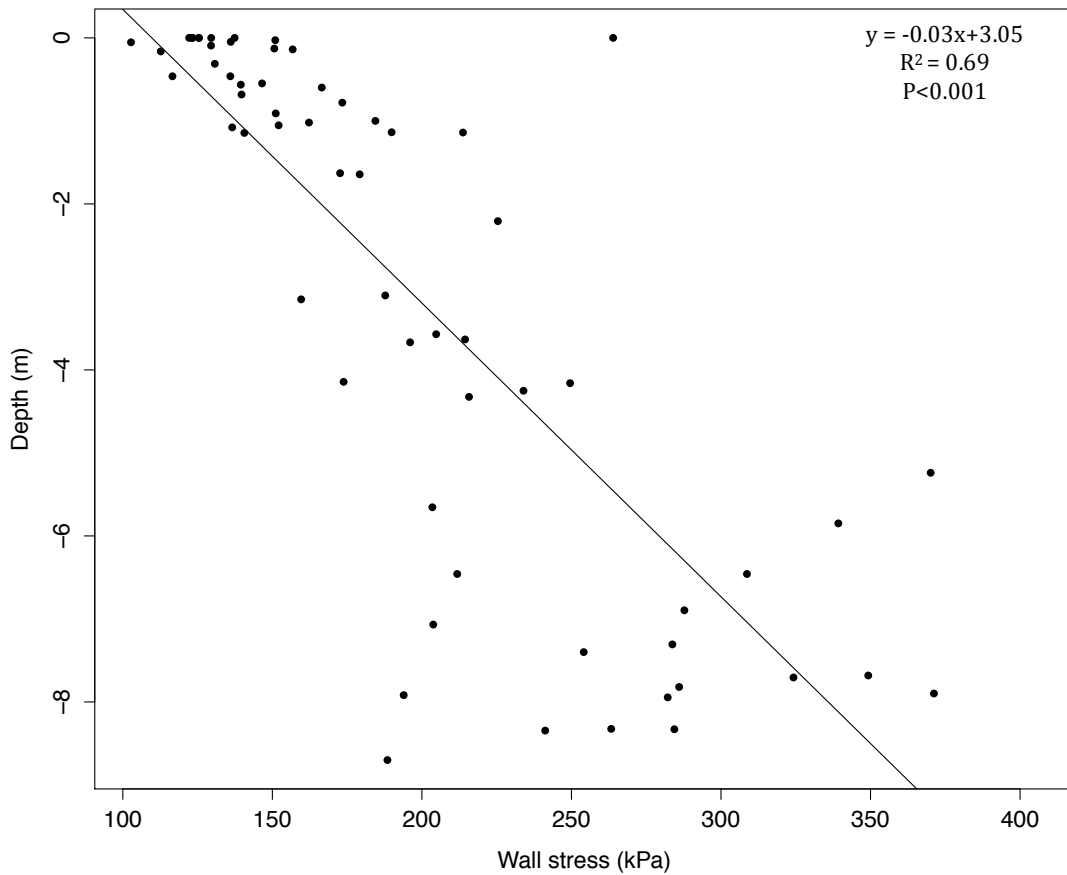


Figure 12: Pneumatocyst wall stress at depths between (0-9 m).

1.3.3 Pneumatocyst wall material properties

The modulus of smaller pneumatocysts (3-50 cm³) varied from 0.9 to 10 MPa (Fig. 13). Modulus increased significantly (up to 12 MPa) as pneumatocyst volume increased from 8 cm³ to 1200 cm³ (Fig. 13; $P < 0.001$, $R^2 = 0.28$).

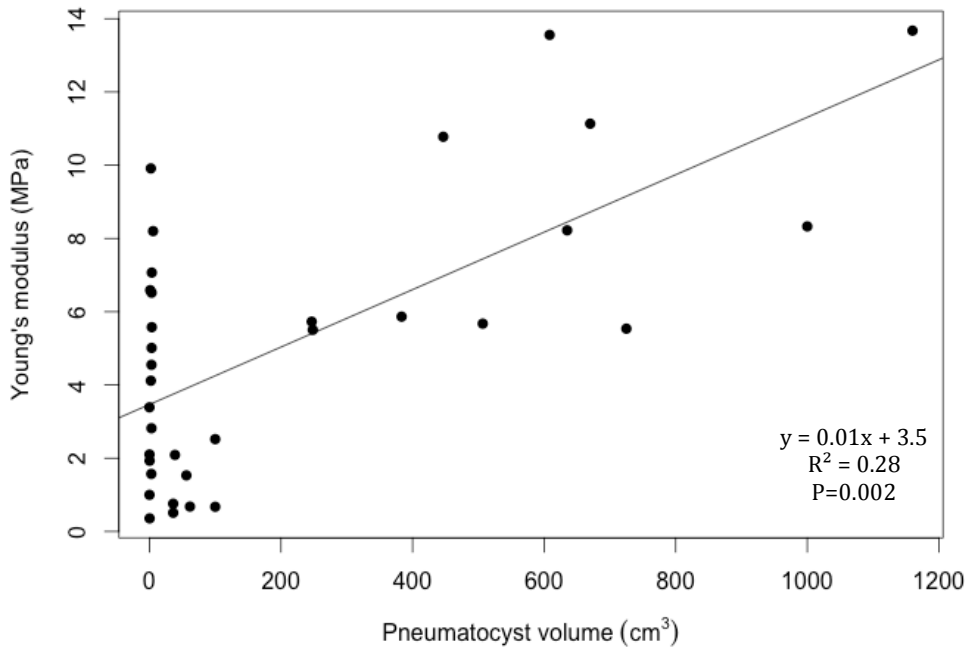


Figure 13: Young's modulus for different pneumatocyst volumes.

1.3.4 Pneumatocyst geometry

According to eqn. 6, wall stress at a given depth increases with increasing inner radius to wall thickness ratios (Fig. 14A). At 6 m of depth, the estimated wall stress increased by 30% when the inner radius to wall thickness ratio increased from 1:1 to 3:1, to 6:1 (Fig. 14A). The pneumatocyst's inner radius to wall thickness ratio varied between 1:1 and 6:1, and did not significantly change with depth (Fig. 14B; $P > 0.05$).

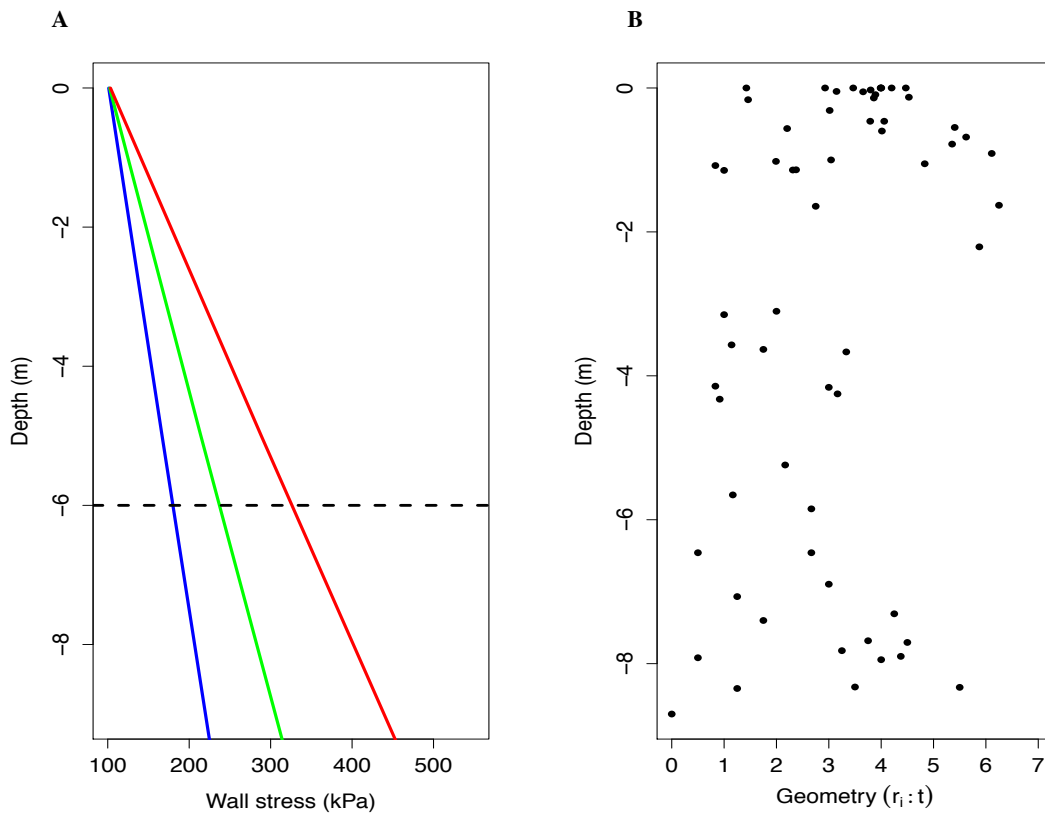


Figure 14: Estimated wall stress at depths from 0-9 m for a given $r_i:t$ ratio (r_i = inner radius, t = wall thickness; 1:1(blue), 3:1(green), and 6:1(red); A). Dashed line indicates estimates of wall stress for a given $r_i:t$ ratio at 6 m. $r_i:t$ ratio at depths between 0-9 m ($P>0.05$; B).

Linear regression analysis indicated that small pneumatocysts at depth (between 7 m and 8.7 m) significantly increased in wall stress (from 187 kPa to 371 kPa) as pneumatocyst geometry ($r_i:t$) increased from 0.5 to 4.4 (Fig. 15; $P<0.001$, $R^2=0.67$).

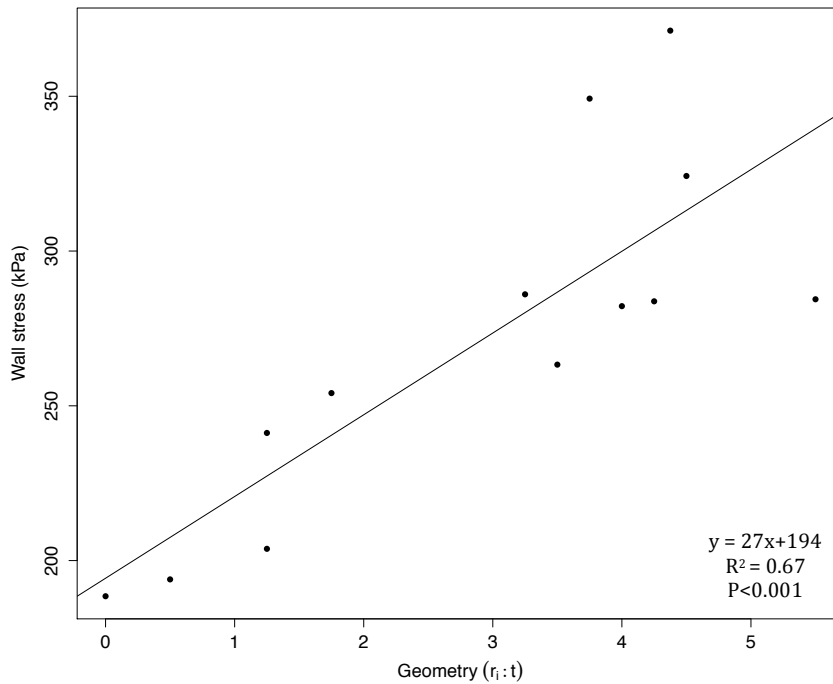


Figure 15: Pneumatocyst wall stresses for small pneumatocysts with different $r_i:t$ ratios. All pneumatocysts were collected between 7 and 8.7 meters.

Inner radius increased from 0 cm to 3.5 cm as pneumatocysts grew from 9 m to 0 m (Fig. 16A). Wall stress increases (from 150 to 400 kPa) when the internal radius was between 0 cm and 1 cm (Fig. 16B). Wall stress decreased from 400 to 150 kPa when the internal radius increased from 1 cm to 2 cm (Fig. 16B). Wall stress remained invariant when the inner radius was greater than 2 cm (Fig. 16B). The ratio between inner radius and wall thickness increased from 0 to 6 as internal radius increased from 0 cm to 3.5 cm (Fig. 16C; $P < 0.001$, $R^2 = 0.48$). Data collected with an inner radius below 1 cm and an $r_i:t$ value around 4 had the highest wall stress values (Figs. 16B-C). Generally an inner radius of 0.8 cm to 0.9 cm and a wall thickness of 0.2 cm had the highest stress values (Fig. 16B; Fig. 16C circled portion). As inner radius increased from 0 cm to 1 cm, the total pneumatocyst tissue volume did not greatly increase (average volume =

$2.3 \pm 1.7 \text{ cm}^3$; Fig. 16D). Pneumatocyst tissue volume then gradually increased from 2.3 cm^3 to 200 cm^3 as the internal radius increased from 1 cm to 3.5 cm (Fig. 16D).

Overall pneumatocyst tissue volume increased by a factor of 142 once the inner radius was greater than 1 cm (Fig. 16D).

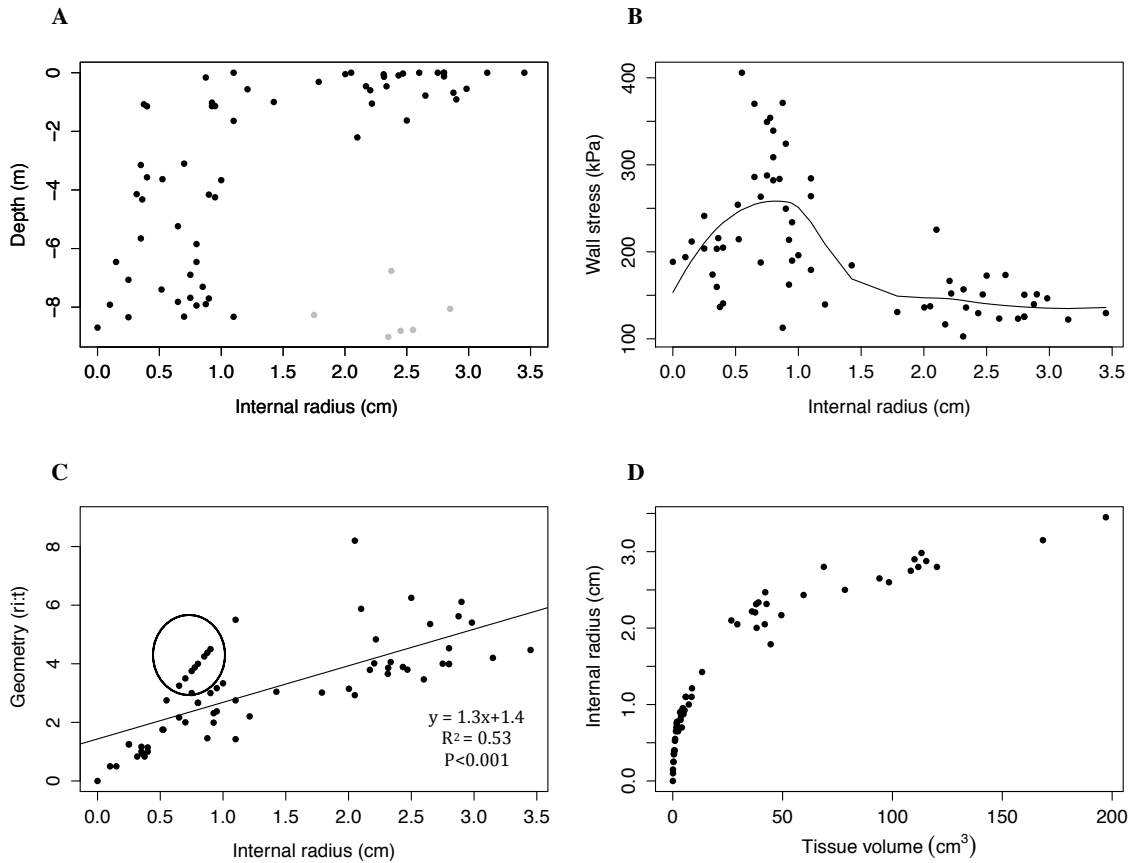


Figure 16: Inner pneumatocyst radius at different depths (A). Grey data points are samples that began growing below 9 m and thus growth data is missing from the substratum to 9 m. These data were not included in analyses of pneumatocyst development. Pneumatocyst wall stress with an inner pneumatocyst radius (B). Black dotted line indicates overall trend in wall stress as inner radius increases. r:t ratio with inner radius from (C). Black circle indicates pneumatocysts with the greatest wall stresses shown in part B. Inner pneumatocyst radius with pneumatocyst tissue volume (D).

1.3.5 Pneumatocyst safety factor

Table 1 shows the calculated Environmental Safety Factor (ESF) of collected pneumatocysts using eqn. 7. Average ESF was 3.9 ± 0.92 (Table 1). Table 2 shows the estimated critical breaking depth and breaking stress of 2 small pneumatocyst with critical geometry ($r_i=0.8-0.9$ cm, $h=0.2$ cm) found between 7 m and 8 m. These pneumatocyst were estimated to break at 21 m and 35 m with a breaking stress of 1263 and 1100 kPa respectively (Table 2).

Collected Depth (m)	σ_0 (kPa)	σ_{break} (kPa)	Depth Break (m)	ESF
2.7	132.8	590.5	16.8	4.4
2.1	136.9	632.8	18.0	4.6
3.5	124.2	470.1	18.0	3.8
6	178.5	464.5	16.8	2.6

Average: 3.9 ± 0.92

Table 1: Table showing calculated ESF values for 4 pneumatocysts collected between 2.7 m and 6 m.

Pneumatocyst	A	B
Depth (m)	7	7.9
r_i (cm)	0.9	0.8
t (cm)	0.2	0.2
Internal pressure (kPa)	86	91
ESF	3.9	3.9
σ_0 (kPa)	324	282
σ_{break} (kPa)	1263	1100
Breaking depth (m)	37	35

Table 2: Estimated critical breaking depth and breaking stress for 2 small pneumatocysts (with critical geometry) recorded to have the greatest wall stresses and the greatest r_i ;t found between 7 m and 8 m of seawater.

1.4. Discussion

1.4.1 Changes in pneumatocyst internal pressure and volume

Unlike a passive balloon, whose volume was expected to increase two-fold as it rose to the surface, pneumatocyst volume increases by a factor of 400 (Fig. 8A). Clearly, *Nereocystis* is expanding more than expected for a passive gas-filled structure, which suggests that the pneumatocyst is not passive but rather increases volume significantly through growth and development. In the absence of mitigating responses, pneumatocyst expansion due to decreasing internal pressure would thin, strain, and potentially weaken the wall. The pneumatocyst overcomes this obstacle, in part, by extending into the stipe and having a meristematic region in the tissue, which allows the wall to become thicker as volume increases (Nicholson 1970; Fig. 2B).

Manometer readings reveal that pneumatocysts consistently have an internal pressure less than atmospheric pressure (Fig. 8B). These results support previous studies showing that older pneumatocysts had internal pressures less than 101 kPa (Langdon 1917; Rigg and Swain 1941). Dromgoole (1981) argued that lower internal pneumatocyst pressures of *Carpophyllum spp.* and *Macrocystis pyrifera* were a result from shading at depth, slowing oxygen production from photosynthesis. But, if this were true, the proportion of O₂ in the pneumatocyst would vary with depth. Results discussed in Ch.2 suggested that there was no significant change in O₂ concentrations as pneumatocysts grew larger and therefore it is unlikely that smaller pneumatocysts have lower pressures due to reduced oxygen production (See Ch.2). Rigg and Swain (1941) suggested the low pressure found in adult pneumatocysts was caused by rapid development, where pneumatocyst volume increases at a rate faster than the gas being put into it. This study

suggests that pneumatocysts continue to have a pressure less than 101 kPa throughout development, supporting the ideas presented by Rigg and Swain (1941).

Since sporophytes start growth at various depths, there are two confounding variables that can affect internal pneumatocyst pressure: depth and volume. To test the effect of depth and to control for the effect of size (volume), I compared small pneumatocysts growing at >8 m depth and <2 m near the surface. At a single size, depth did not have a significant effect on pressure, and thus it is likely internal pressure changes independently of changing depth (Fig. 9).

As sporophytes grow and pneumatocyst volume increases, internal pressure and the total amount of gas reach an asymptote (Fig. 10). Young pneumatocysts have variable internal pressures and total gas. Although the sample size for large pneumatocysts (>200 cm³) is low, these data indicate that internal pressure becomes closer to 80 kPa as pneumatocysts grow in size. According to the Ideal Gas Law (shown in eqn. 5), gas molecules released into the developing pneumatocyst would directly influence its internal pressure. Thus, as suggested by Rigg and Swain (1941), though gas is being added to the pneumatocyst as it becomes larger, the pressure is still below atmospheric pressure due to a rapid increase in volume. It is also possible that pressure is controlled and deliberately held at 80 kPa to ensure that the material stays in compression, as the force differential decreases during pneumatocyst development. If internal pressure is higher than outer ambient pressure, the pneumatocyst material would need to be capable of tolerating tension. Since the material is already built to tolerate compression, it would likely be less cumbersome to continue resisting compression rather than producing a material that tolerates 2 different types of loads.

In sum, these data suggest that pneumatocyst internal pressure is not influenced by depth as it grows towards the surface, but rather changes in volume directly affect the internal pressure. Therefore when a sporophyte begins its life at depth, internal pressure changes at a rate slower than its rapidly growing pneumatocyst. These results reveal that pneumatocysts are not passive but rather actively regulated, and biological processes such as photosynthesis, respiration, and gas composition attribute to lower pressures found in pneumatocysts (See Ch.2).

1.4.2 Pneumatocyst wall stress and the risk of buckling

Contrary to what we expected in the balloon model, the risk of breaking decreases as pneumatocysts move towards the surface. Because internal pneumatocyst pressure is less than external hydrostatic pressure, pneumatocysts are constantly exposed to a positive pressure gradient (ΔP ; Fig. 11) and therefore always under compression. The difference in external hydrostatic pressure and internal pneumatocyst pressure becomes greater with depth (Fig. 11), resulting in younger, smaller pneumatocysts experiencing the greatest loads and greatest risk of buckling.

Furthermore, since the pressure gradient is positive, the pneumatocyst experiences compressive forces at every stage of development. Thus under compressive forces, pneumatocysts can be at risk of buckling as the pressure gradient increases, making the average wall stress increase with depth (Fig. 12). The contribution of pneumatocyst geometry also does not prevent changes in material stress with depth (Fig. 14B), and thus pneumatocysts that are found at depth are at greatest risk of buckling. As mentioned previously, deeper pneumatocysts tend to be small and young, therefore sporophytes

reach a critical survival point early in their development, where success in reaching adulthood depends on either tolerating or reducing material stress.

1.4.3 Reducing wall stress

Variation in overall geometry ($r_i:t$) (Fig. 14B), less stiff materials (Fig. 13), and higher wall stress at depth (Fig. 12), suggests that young pneumatocysts could be at risk of buckling. Though the elastic modulus of seaweed tissues generally varies with species and habitat (Dromgoole 1981), previous studies have suggested that a large change in material modulus (stiffness) would be needed to resist breaking as a pneumatocyst increases volume (Charters et al. 1969; Delf 1932). Therefore, if *Nereocystis* pneumatocyst materials were adjusted to resist buckling, modulus would need to be greatest at depth to reduce strain or deformation from elevated wall stress. Contrary to this speculation, the pneumatocyst wall has a modulus that was lowest in young individuals and becomes stiffer as volume increases (Fig. 13). Since pneumatocyst material stress is greatest at depth, changes in the material's modulus does not reduce wall stresses. Furthermore, if *Nereocystis* were adjusting pneumatocyst morphology to reduce stress, then $r_i:t$ would be smallest at depth where material wall stress and the risk of buckling is greatest. However, $r_i:t$ ratios of deep pneumatocysts vary from 1:1 to almost 6:1 and do not correlate with depth (Fig. 14B), which suggests that pneumatocysts do not adjust their geometry to reduce wall stress.

1.4.4 Pneumatocysts at risk of buckling

How then do pneumatocysts resist buckling? The present study demonstrates that $r_i:t$ increases during development (Fig. 16C). Dromgoole (1981) suggested that a decline in $r_i:t$ would potentially make older pneumatocysts more susceptible to buckling under hydrostatic pressure. However, data presented here argue against this idea for two reasons. First, pneumatocyst inner radius increases as thalli grow toward the surface and therefore larger pneumatocysts are not found at depth (Fig. 16A). This is because the stipe elongates, moving the developing pneumatocyst towards the surface. Second, pneumatocyst wall stress is generally decreases once the pneumatocyst reaches an inner radius greater than 1 cm (Fig. 16B). During stipe elongation, the pneumatocyst experiences decreasing hydrostatic pressure, contributing to the overall reduction of wall stress. This previously mentioned concept presented by Dromgoole (1981) could be applied to pneumatocysts that are ‘stationary’ and experience similar hydrostatic pressures throughout development. However, since the pneumatocysts of *Nereocystis* experience decreasing hydrostatic pressures as they develop, Dromgoole’s concept cannot be applied.

The critical buckling geometry during the life of a developing pneumatocyst is when the inner radius is around 0.8 cm - 0.9 cm and the wall thickness is around 0.2 cm (Figs. 16B-C). This geometry is considered critical since the pneumatocyst has a $r_i:t$ around 4:1 and the greatest amount of material stress, about 300 kPa (Figs. 16B-C). These values reflect that the particular geometry of this pneumatocyst is not being utilized to reduce overall wall stress. Material stress tends to be greatest in small pneumatocysts with a $r_i:t$ ratio around 4:1 (Fig. 15). This increase in material stress is due

to $r_i:t$ increasing beyond a geometry of 1:1 (Fig. 15; Fig. 16C). These changes in $r_i:t$ suggest inner radius increases and the pneumatocyst wall does not thicken (Figs. 16B-C). Therefore during this point in development, pneumatocyst tissue volume does not change as internal radius increases, and as a consequence, wall stress increases (Fig. 16B; Fig. 16D). A pneumatocyst generally reaches this critical size immediately after formation, when there is little to no change in the total pneumatocyst tissue volume. At this point, gas begins to fill the very small torn pneumatocyst space, separating the medullary tissue to form the pneumatocyst wall (Fig. 16D). These results indicate that pneumatocysts can experience critical breaking stresses early in development at depth. During pneumatocyst formation, individuals need be capable of tolerating these critical stresses since the force differential, material properties, and geometry do not aid in reducing stress. If the young pneumatocyst is not able to withstand these compressive forces, the structure will be compromised and it is unlikely that the sporophyte would reach adulthood.

1.4.5 At what depth will a small pneumatocyst break?

Small pneumatocysts found at depth with the critical geometry is estimated to tolerate material stresses up to 35 m of seawater (Table 2). Theoretically, if a young pneumatocyst had no material imperfections or geometric discontinuities, the critical breaking pressure using eqn. 2 (and a modulus of 3.9 MPa; Fig. 13) would be between 31 m and 36 m. These estimates assume that the pneumatocyst material has a Poisson's ratio of 0.3. Current estimates of buckling pressure calculated from eqn. 6 and eqn. 7 are reasonably close to values of critical buckling pressure from eqn. 2 (Table 2). Similarities between these theoretical projections and the actual stress calculations indicates eqn. 6

truly represents the structural design and compressive loads a young pneumatocyst would experience.

Generally, pneumatocysts have an average safety factor of 3.9, suggesting that pneumatocysts are about 4 times stronger than they need to be (Table 1). We can estimate if a pneumatocyst at the critical moment in its life is at risk of buckling by calculating its breaking stress and depth. A young pneumatocyst with the hypothesized (mentioned previously) critical geometry of $r_i = 0.8-0.9$ cm and $t=0.2$ cm, will experience 1100 to 1200 kPa of wall stress at the point of buckling (Table 2). These pneumatocysts are then estimated to buckle in about 35-37 m of seawater (Table 2). These predicted buckling depths are remarkably similar to the maximum observed depth of *Nereocystis* (Spaulding and Foster 2003). Spaulding and Foster (2003) suggested the depth limitation of a growing sporophyte was due to light availability. The present study demonstrates that hydrostatic pressure, not just light attenuation, might also define the lower limit of *Nereocystis* in the field.

1.4.6 Conclusion

This study demonstrates how the pneumatocyst of *Nereocystis* is not passive like a balloon. As pneumatocysts move from depth towards the surface, volume increases 400 fold while internal pressure does not significantly change. However, the increase in pneumatocyst volume causes internal pressure to be less than ambient air pressure. Internal pressure is variable in younger pneumatocysts and begin to reach 80 kPa as they become adults. Therefore, internal pressure tends to be less than atmospheric pressure, possibly because the pneumatocyst develops at a rate faster than the gas being added.

Pneumatocysts have an internal pressure less than the hydrostatic pressure they are exposed to. This results in a positive pressure gradient and therefore young pneumatocysts experience compressive forces throughout development. This positive pressure gradient increases with depth, which suggests that young, small pneumatocysts experience the greatest compressive loads, putting them at greatest risk of buckling.

Pneumatocyst material properties and geometry ($r_i:t$) are not optimized to reduce wall stress and do not help reduce the risk of buckling. Furthermore, wall stress is greatest in young pneumatocysts that have an inner radius between 0.8-0.9 cm and wall thickness of 0.2 cm ($r_i:t \sim 4$), revealing a critical size (directly after formation) where the pneumatocyst is at greatest risk of buckling. Pneumatocysts are approx. 4-times stronger than they need to be to resist buckling. Theoretical and calculated estimates in this study indicate that small pneumatocysts will buckle at approximately between 31 m and 37 m depth. These data suggest that hydrostatic pressure, not just light limitation may contribute to the maximum depth of pneumatocysts. In the future, critical buckling pressure should be measured on young pneumatocysts to verify predictions from this study.

Chapter 2

Developmental changes in gas composition and buoyancy of

Nereocystis pneumatocysts

2.1 Introduction

2.1.1 Growth and development

Nereocystis luetkeana (*Nereocystis*) provide marine habitats for an array of organisms in near shore environments (Nicholson 1970). This kelp creates dynamic subtidal forests (Arzee et al. 1985) that are upright and extend from 35 m deep towards the surface of the sea. Subtidal kelps use one of two strategies to remain upright in the water: Some species maintain an upright stature by having a tough, rigid stipe, and others, like *Nereocystis* have a flexible thallus with buoyant, gas-filled floats called a pneumatocysts. Buoyant pneumatocysts keep the flexible seaweeds vertical in the water.

At 10-35 m depth, young sporophytes start their life in an environment with little light (Spalding et al. 2003). During pneumatocyst development, medullary cells along the transition zone begin to tear, releasing gas and creating the pneumatocyst (Dromgoole 1981). Once the pneumatocyst has formed, the sporophyte begins to grow rapidly towards the surface (Duncan 1973). As thalli become larger, they also increase biomass and become heavier, having blades that can weigh up to 20 kg in air (Denny et al. 1997). Sporophytes are able to grow towards the surface by adding gas to the developing pneumatocyst, which ultimately increases buoyancy (Kain 1987).

2.1.2 Pneumatocyst gas composition and production

Gas composition and internal pressure of pneumatocysts were heavily studied in the early 20th century (Frye et al. 1915; Langdon 1917; Langdon and Gailey 1920; Zeller and Neikirk 1915.). These studies concluded that 20- 25% of gas sampled from pneumatocysts was oxygen (O₂) and about 70% or more was nitrogen (N₂) (Langdon 1917; Rigg and Swain 1941), with both gases present in concentrations similar to air. Up to 13% carbon monoxide (CO) (Langdon and Gailey 1920) and about 2-7% carbon dioxide (CO₂) were also documented from pneumatocysts.

Pneumatocysts become thicker with age, making gas loss unlikely, and thus all gases produced throughout development are stored (Langdon 1917; Langdon and Gailey 1920). Pneumatocyst volume increases at a rate faster than gases are produced, resulting in an internal pressure that is less than hydrostatic pressure (negative pressure) (Frye et al. 1915; Rigg and Swain 1941; See Ch.1). Pneumatocysts are able to regulate the production of internal gas and therefore internal pressure (Brackenbury and Garbary 2006). As a result, the partial pressure of gases drives the overall internal pressure inside the pneumatocyst.

In macroalgae, nutrient uptake generally correlates with the surface area of the thallus per unit volume (surface area:volume ratio or SA:V) (Rosenberg & Ramus 1984; Taylor et al. 1998; Hein et al. 1995). Similarly, gas production may correlate with the SA:V ratio of cells that line the inner wall of the pneumatocyst. Throughout sporophyte development, pneumatocyst SA:V decreases as pneumatocysts become larger. In other words, the number of cells in one cubic centimeter decreases as pneumatocyst volume increases, since cells in the pneumatocyst begin to elongate (Duncan and Foreman 1980).

If the gases in the pneumatocyst are a product of surface area, then as pneumatocyst volume increases, the concentration (%) of biologically-produced gases will also decrease; this would result in a large pneumatocyst that is mostly filled with inert N₂, with a gas composition similar to air (NOAA.com, USA). Pneumatocyst gas composition has only been studied in adult sporophytes, and has never been adequately quantified throughout development. As mentioned in Ch.1, internal pneumatocyst pressure actually increases as pneumatocysts become larger. It is therefore possible that the total amount of gas increases as pneumatocysts become larger, but that the overall gas composition changes.

By conducting in-situ experiments, Rigg and Swain (1941) demonstrated that internal pressure of large pneumatocysts fluctuates, reaching a maximum around the late afternoon when pneumatocyst cells have been exposed to light for an extended period of time. Pressure reaches a minimum during the night when light is no longer available (Rigg and Swain 1941). Though Rigg and Swain (1941) only measured the physiological gas composition of adult pneumatocysts (~1000 ml), these fluctuations could likely change in magnitude due to changes in SA:V as pneumatocysts develop. However, no one has ever measured changes in gas composition and pressure concurrently in pneumatocysts of various sizes. If the pressure depends upon activity of the pneumatocysts' physiologically active cells, then the magnitude of pressure fluctuations should change as SA:V decreases with increased pneumatocyst volume.

2.1.3 Pneumatocyst buoyancy

According to Archimedes principle, any object completely or partially immersed in a fluid is buoyed up by a force equal to the weight of the fluid displaced by the object. Since salt water is approximately 1000 times more dense than pneumatocyst gases, buoyant force can be generated by the pneumatocyst as it displaces seawater. As the pneumatocyst increases in volume, more water is displaced, creating an upward buoyant force that keeps the flexible thallus upright.

Nereocystis have a large thallus that is more dense than seawater, posing potential problems as the dense tissue becomes heavier with increased size. These heavy thalli can weigh up to 20 kg in air, creating a substantial negative force that acts against the pneumatocyst (Denny et al. 1997). The pneumatocyst can no longer support the flexible thallus if its positive buoyant force is less than or equal to the weight of the tissue in seawater. It is important that the increase in pneumatocyst volume paces or outpaces the increase in thallus mass as *Nereocystis* grows. If the pneumatocyst is unable to support the heavy thallus, the sporophyte is at risk of sinking. If pneumatocyst buoyancy is increased at a rate greater than the mass being added to the sporophyte, then it could potentially waste energy by producing excess gases. Ideally, the sporophyte should increase pneumatocyst buoyancy at a comparable rate to the increase in mass during growth.

2.1.4 Study objectives

In this study, I measured total gas composition of *Nereocystis* pneumatocysts of varying sizes. This allowed me to determine if pneumatocyst gas composition changes

during pneumatocyst development and growth. Since pneumatocyst SA:V decreases as pneumatocysts become larger, I predicted that the total proportion of physiological gases also decreases as pneumatocysts develop, leaving a pneumatocyst that is mostly comprised of N₂. Using pneumatocysts of different sizes, I repeated experiments conducted by Rigg and Swain (1941), and investigated the diurnal changes in internal pneumatocyst pressure and CO₂ in-situ in order to determine how gas fluctuations are influenced by changes in SA:V during development.

It is well known that pneumatocysts are used to produce an upward buoyant force, keeping the thallus upright in the water. In this study, I determined whether or not the buoyant force of the pneumatocyst changes to compensate for the fast growing thallus. I investigated if buoyancy is maintained by calculating the buoyant safety factor (BSF) for different life stages of the sporophyte. I also investigated whether the pneumatocyst's BSF is maintained or changes with increased thallus size.

2.2 Methods

2.2.1 Specimen collection

Nereocystis thalli (n = 31) of various sizes were collected in Bamfield, British Columbia Canada, at three locations: Scott's Bay (48.834687, -125.147232), Aguilar Point (48.839456, -125.140896), and Helby Island (48.855442, -125.168718; Fig. 17). Plants were collected no deeper than two meters below chart datum. All samples were detached from the substratum at the holdfast so that pneumatocysts were fully intact. All specimens were taken back to the Bamfield Marine Sciences Centre for further evaluation. After experimentation, pneumatocyst volume was measured by carving a hole

in the pneumatocyst, filling the inside with water and pouring it into a graduated cylinder. An average of 3 measurements was used to determine volume. Pneumatocyst length and width was measured using a measuring tape (mm). Pneumatocyst wall thickness was measured using calipers (mm). All statistical analyses were conducted using R version 0.99.467 (R Core Development Team).

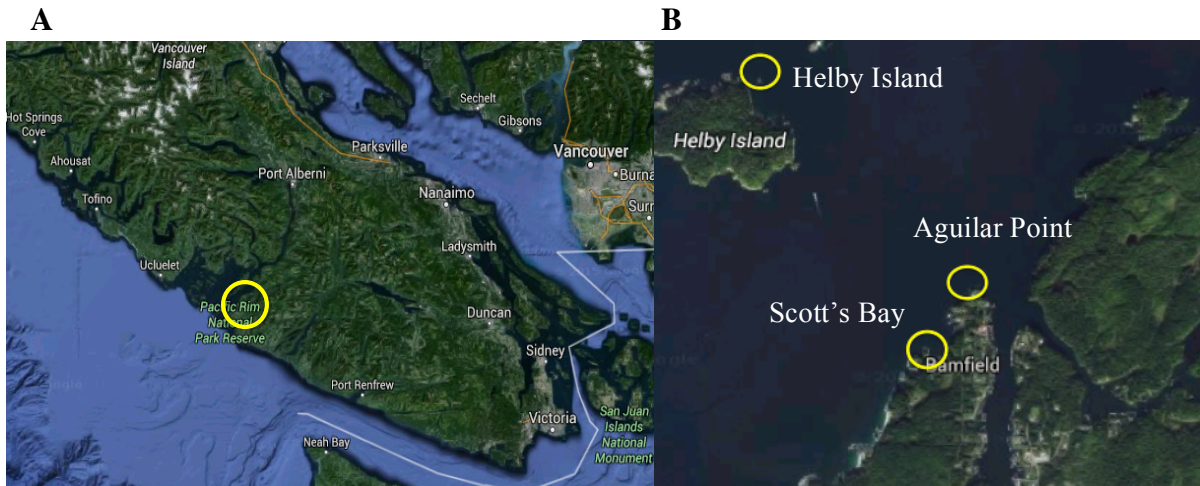


Figure 17: Map of southern Vancouver Island, British Columbia Canada. The yellow circle indicates location of Bamfield (A). Map of field sites where *Nereocystis* was collected (B) (provided by Google Maps).

2.2.2 Internal gas composition

12 ml of gas was extracted with a 26 gauge (0.45 mm) needle and syringe from each pneumatocyst and stored in an Exetainer (Labco Limited 12ml, Lampeter UK). All Exetainers were vacuumed sealed and contained a septum to allow gas to be stored without air contamination. Exetainers were punctured no more than 3 times to avoid air contamination (Glatzel and Well 2008). Each Exetainer was stored upside down in distilled water to further prevent air contamination (Sturm et al. 2015). Samples were cooled to 5°C during transit and in the lab prior to gas analyses.

CO₂ and CO concentrations in gas samples extracted from pneumatocysts were analyzed at room temperature (in ppm) using a Q-trak indoor air quality monitor 7565 (TSI Inc. MN USA). Q-trak sensors were calibrated to 50 ppm of CO and 447 ppm of CO₂ (CO₂ in air) using a plastic case (calibration wand) that covered the sensors on the Q-Trak wand (Fig. 18). The calibration wand was also used in gas analyses by attaching rubber tubing at the end of the wand injecting 0.5 ml pneumatocyst samples through the tubing. CO₂ and CO was electronically read after the gas sensor ran for 45 seconds, recording a peak concentration. N₂ was used to flush out any excess air in the sensor that would alter measurements.

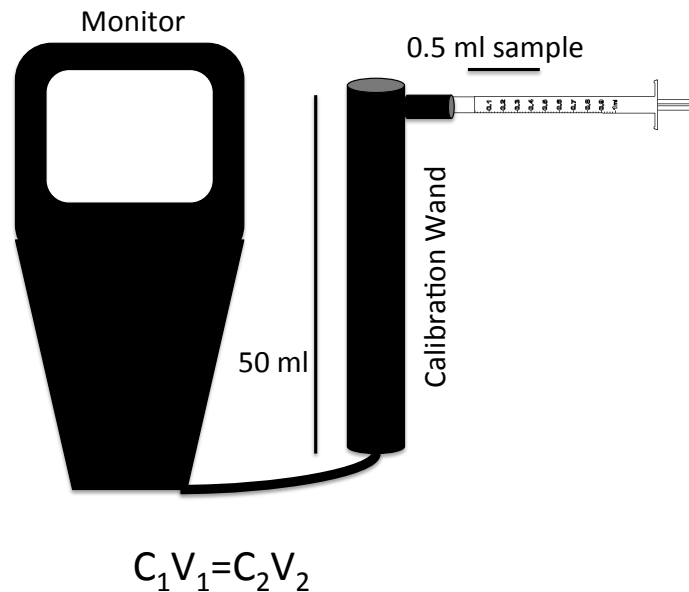


Figure 18: Diagram of Q trak sensor. CO₂ and CO concentrations in the pneumatocyst were calculated using the equation above. Where C₁ = the concentration read on the monitor (ppm), V₁ = volume of the calibration wand (ml), C₂= unknown pneumatocyst concentration (ppm), and V₂= 0.5 ml sample.

Neofox probes (Ocean Optics Inc. FL USA) were used to measure O₂ concentrations in gas samples extracted from pneumatocysts (in %) diluted in a 50 ml sealed flask. Before each measurement, the flask was flushed with 100% N₂ to evacuate

any residual air. The flask had two openings, one of which was sealed using tape after the N₂ flush, while the other was sealed by placing the Neofox probe into the flask, using tape to place a final seal around both openings. 2 ml of gas was extracted from the Exetainers using a 26 gauge (0.45 mm) needle and was placed into the flask with the probe. Each sample was mixed with the residual N₂ using a magnetic stir bar during the reading. Data was recorded by measuring the peak concentration of O₂ as the gas sample mixed with residual N₂. Total gas concentration (ppm) of each sample was calculated using the following equation:

$$C_2 = \frac{C_1 V_1}{V_2} \quad (8)$$

Where C₁ = the measured gas concentration (ppm), V₁ = volume of the flask (50 ml), C₂ = unknown pneumatozyst concentration (ppm), and V₂ = 2 ml gas sample (ml). The same equation was used to calculate total CO and CO₂ concentration in the pneumatozyst where C₁ = concentration measured from the 0.5 ml sample.

Gas concentrations (ppm and %) were plotted against pneumatozyst volumes and fitted with linear regressions. Log-transformed total gas (mmol) were plotted against pneumatozysts volume, and significant correlations were tested using linear regressions.

2.2.3 Pressure and CO₂ fluctuations

Nereocystis (n = 12) were collected from Scott's Bay from July 8 - 11, 2015 and stored in outdoor seawater bins with continuous flowing seawater between 11 and 13°C. Nine pressure manometers (diameter: 4-8 mm; length: 20-60 cm; Fig. 19) were placed vertically at a 90 degree angle on each bin. Experimental bins were side-by-side and exposed to direct sun with limited potential shading over the course of the day.

For each round of experiments, pneumatocyst sizes varied from 5 to 400 ml. All samples were prepared by tying twine to the stipe and gluing it to the lip of the tank. This allowed for constant water flow without samples moving in the tank. Rocks were attached to help holdfasts to maintain the vertical posture they exhibit in their natural environment. The vertical posture also limited the effect of shading, allowing the full photosynthetic area to be exposed. Pneumatocysts were punctured with a 21 gauge (0.7 mm) needle and equalized to atmospheric pressure so that the changes in pressure and CO₂ would only reflect gas production and utilization of pneumatocyst cells. Water manometers were attached to pneumatocysts using plastic tubing, syringes, and needles (Fig. 19).

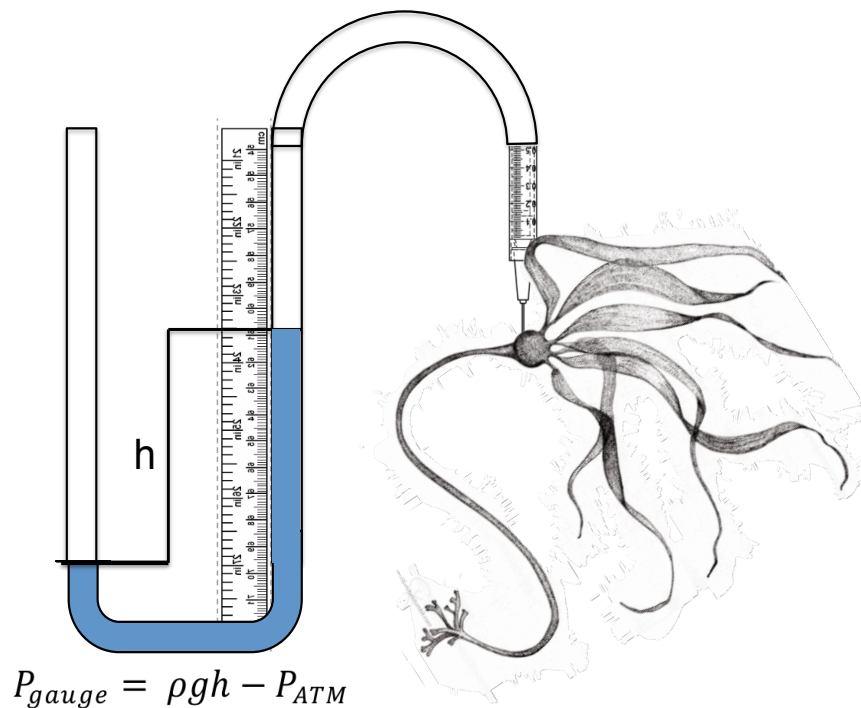


Figure 19: Diagram of water manometer. Pneumatocysts were punctured using a lubricated syringe needle. Gauge pressure was calculated by the equation above where ρ = density of water 1025 kg m^{-3} , $g = 9.81 \text{ ms}^{-1}$, h = height of water moved in both arms post puncture, and P_{ATM} = atmospheric pressure.

Pneumatocysts were towel-dried before puncturing and the inserted needle was sealed with super glue and Vaseline. Initial pressure readings were recorded an hour after the pneumatocysts were punctured. Internal pneumatocyst pressure was then calculated by using the dimensions of the manometer and the Ideal Gas Law to derive eqn. 9:

$$\begin{aligned}
 P_{\text{gauge}} V_{\text{total}} &= nRT \quad (\text{Ideal Gas Law}) \\
 &= (n_{\text{Pn}} + n_{\text{mi}})RT \\
 &= \left(\frac{P_{\text{Pn}} V_{\text{Pn}}}{RT} + \frac{P_{\text{mi}} V_{\text{mi}}}{RT} \right) RT \\
 &= P_{\text{Pn}} V_{\text{Pn}} + P_{\text{mi}} V_{\text{mi}} \\
 P_{\text{Pn}} &= \frac{P_{\text{gauge}} V_{\text{total}} - P_{\text{mi}} V_{\text{mi}}}{V_{\text{Pn}}} \quad (9)
 \end{aligned}$$

$$\text{Where } V_{\text{total}} = V_{\text{Pn}} + V_{\text{mf}}$$

where P_{Pn} is the unknown pneumatocyst pressure, P_{gauge} is the pressure reading from the manometer, V_{mf} is the total volume of the manometer from the water line to the needle after the pneumatocyst was punctured, P_{mi} is the pressure of the ambient air in the manometer, V_{mi} is the volume of the manometer arm before the pneumatocyst is punctured, and V_{Pn} is the volume of the pneumatocyst.

Every 4 hours, starting at 21:30, pressure (P_{total}) was measured using the manometer and a 1mL gas sample was extracted using a 21 gauge (0.7 mm) needle and syringe. Each time the pneumatocyst was punctured for a gas sample, the punctured area was sealed using Vaseline. CO_2 concentration was measured in the gas sample by injecting the gas into plastic aquarium tubing (diameter: 4mm; length 10 cm) attached to an A S157 CO_2 Analyzer (Qubit Systems Research, ON Canada), calibrated up to 2000 ppm. Six paired pressure and gas samples were taken for each pneumatocysts over

24 hours. Light intensity and water temperature were recorded at each sampling time using a LI-250A light meter (LI-COR Inc. NB, USA) and aquarium thermometers.

SA:V was estimated for pneumatocysts of various sizes by using previously collected volumes and inner radii of the spherical top (see Ch.1). These estimates were then plotted with previously collected pneumatocyst volumes and log transformed. A linear regression analysis was then performed with the transformed data. The projected linear equation suggested by the regression model was then used to further estimate the SA:V of the pneumatocysts used in this experiment. Recorded amplitudes of the minimum and maximum concentrations of CO₂ was plotted with estimated SA:V to determine if SA:V influences diurnal pressure and gas fluctuations. An average and standard deviation across all 12 samples was also calculated for both internal pressure and CO₂ during each sampling time. Light intensity ($\mu\text{Mol ms}^{-1}$) was plotted with time (24 hour clock starting from 21:30). Both internal pneumatocyst pressure and CO₂ concentration were plotted with time (24 hour clock starting from 21:30).

2.2.4 Buoyant force

Nereocystis thalli (n = 26) were collected from Scott's Bay and transported to the Bamfield Marine Sciences Centre. Stipe and blade densities were calculated by dropping tissue fragments (n= 26) of known mass into a graduated cylinder to measure volume as water displacement, and then by dividing mass by volume. Thallus mass was measured by hand-drying all blades and stipe and weighing them on a 100 kg scale. Thallus volume was calculated by dividing tissue mass by density. Thallus weight in water was then calculated using the following equation:

$$W_{th} = Vg(\rho_{kelp} - \rho_{water}) \quad (10)$$

Where W_{th} is weight of the thallus in water (N), V is the volume of plant (m^3), g is the gravity ($9.81ms^{-1}$), ρ_{kelp} is the density of kelp (kgm^{-3}), and ρ_{water} is the density of seawater ($1025 kgm^{-3}$).

Net buoyancy was measured as the upward force exerted by the whole kelp. Force was measured with a single beam 5 kg force transducer (model #FORT5000, World Precision Instruments Inc. FL, USA) mounted to a basket (Fig. 20).

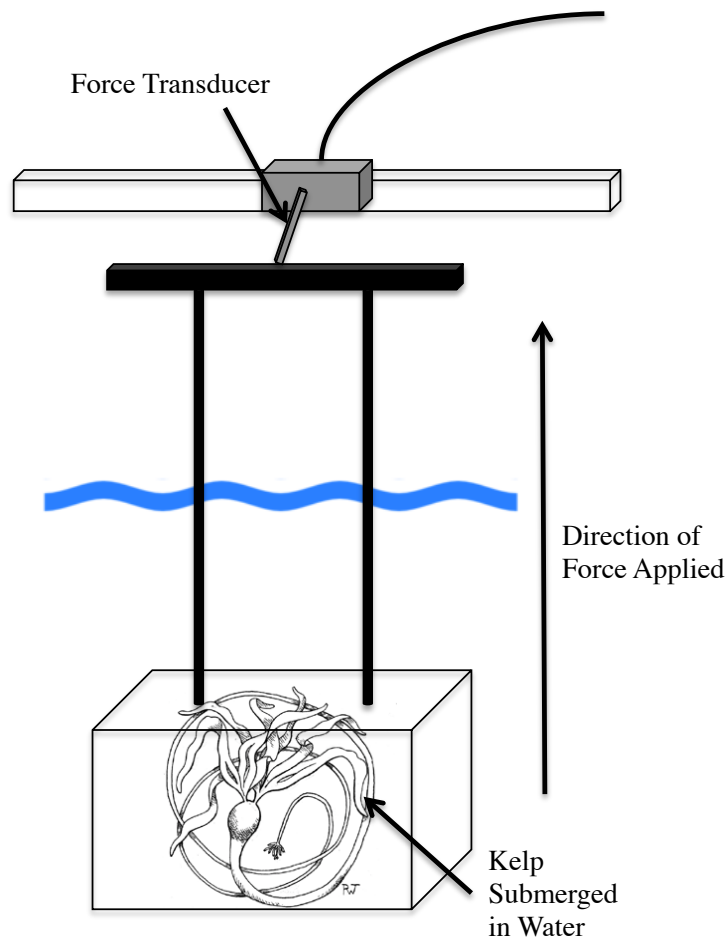


Figure 20: Diagram of contraption designed to measure net buoyant force of the intact thallus. Whole kelp is placed in basket and applies an upward force that is detected by a force transducer.

Measurements were recorded using Lab View/Signal Express. Total buoyant force of was then calculated using the following equation:

$$B_{\text{force}} = B_{\text{net}} + W_{\text{th}} \quad (11)$$

where B_{net} is the net buoyancy (N), B_{force} is the total buoyant force (N), and W_{th} is the weight of thallus (N). Log-transformed weight of thallus in seawater, log-transformed net buoyancy, and log-transformed total buoyant force were plotted against pneumatocyst volumes, and significant correlations were tested using linear regressions.

2.2.5 Buoyant safety factor

Calculating an environmental safety factor (in this context, a buoyant safety factor, BSF) is a method to understand if the pneumatocyst is at risk of sinking at any point during sporophyte development. Generally, environmental safety factor is a ratio of the maximum force a structure can withstand to the force it experiences naturally (Johnson and Koehl 1994; Stewart 2006). A pneumatocyst that has a total buoyant force slightly greater than the weight of the thallus, would have a buoyant safety factor (BSF) slightly greater or equal to one. Any more tissue weight added (i.e. blades), results in the pneumatocysts' total buoyant force equaling the thallus weight, making the sporophyte sink or become neutrally buoyant.

The same 26 *Nereocystis* samples used to measure buoyant force were also used to calculate Buoyant safety factor (BSF). Buoyant safety factor (BSF) was calculated as the ratio between buoyant force and weight of thallus, such that

$$\text{BSF} = \frac{B_{\text{force}}}{W_{\text{th}}} \quad (12)$$

Where B_{force} is the total buoyant force (N) which equals the maximum thallus weight (N) when the pneumatocyst is neutrally buoyant, and W_{th} is the actual weight of the thallus in seawater (N).

5 additional thalli with pneumatocyst volumes between 800 and 1000ml were collected around docks at the Bamfield Marine Sciences Centre. Thallus mass and weight in seawater was measured as mentioned above for all samples. Thallus volume was calculated by dividing tissue mass by density. Maximum weight that pneumatocysts could support before sinking (W_{max}) was calculated by attaching 500 g or 200 g analytical weights on the blades with sewing twine, until the pneumatocyst obtained neutral buoyancy. BSF was calculated using the following equation:

$$ESF = \frac{W_{Max}}{W_0} \quad (13)$$

Where, W_0 is the actual weight of the thallus in seawater (N), and W_{Max} is the added weight (N) attached to the blades and the thallus weight to obtain neutral buoyancy.

Log-transformed BSF for both the original 26 samples and the additional large 5 thalli were plotted against log-transformed pneumatocyst volume, and significant correlations were tested using a linear regression.

2.3 Results

2.3.1 Pneumatocyst gas composition

Relative gas composition did not change significantly with pneumatocyst volumes from 5 to 1000 ml ($P > 0.05$; Figs. 21A-D). Average % concentration for CO, CO₂, O₂, and estimated N₂ were $1.2 \pm 0.78\%$, $0.6 \pm 0.15\%$, $60 \pm 17.2\%$, and $40 \pm 13.7\%$, respectively. Average concentration of CO, CO₂, O₂, and estimated N₂ were 12000, 6000, 590000, and 390000 ppm, respectively (Figs. 21A-D).

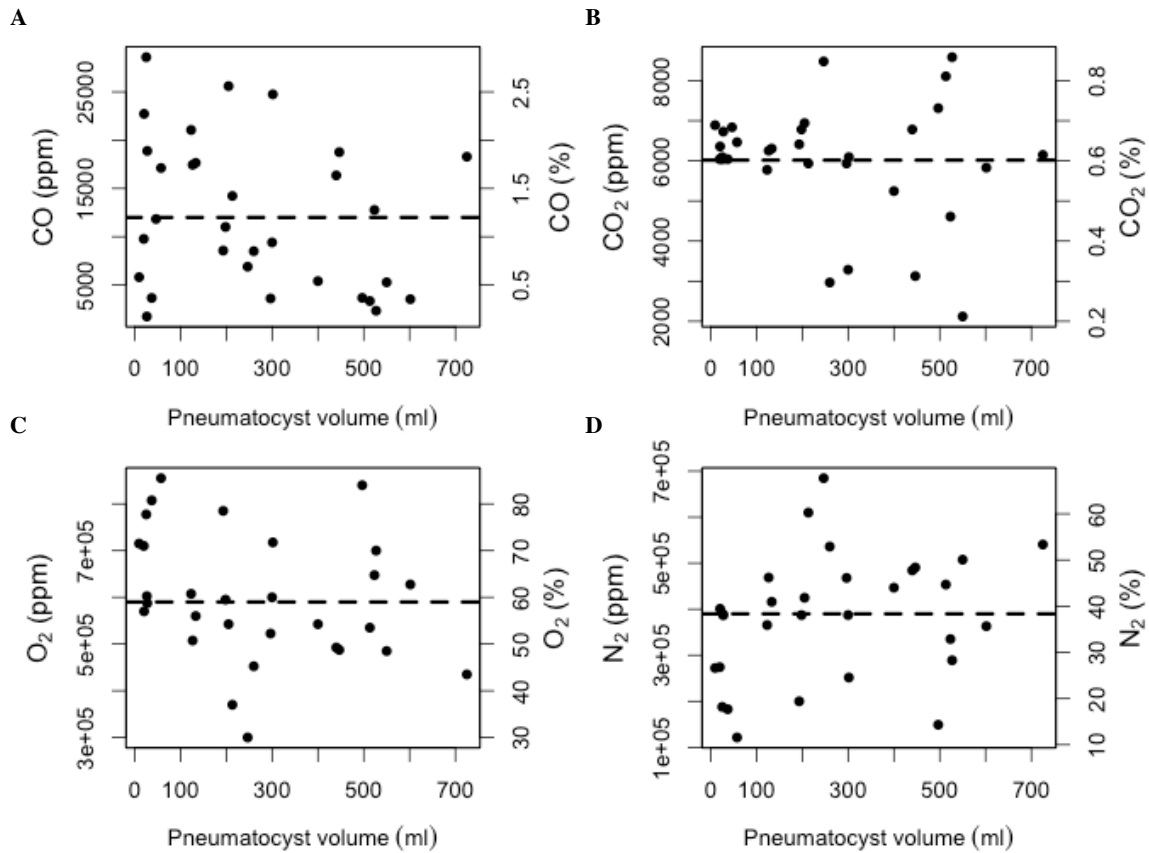


Figure 21: Concentrations of CO, CO₂, O₂, and estimated N₂ for different pneumatocyst volumes (P>0.05). Dotted lines indicate average gas concentration.

However, as pneumatocyst volume increased from 10 ml to 1000 ml, the amount of CO increased significantly from 0.002 mmol to 0.55 mmol ($P < 0.001$, $F = 61.93$, $R^2 = 0.68$; Fig. 22A); CO₂ increased significantly from 0.003 mmol to 0.19 mmol ($P < 0.001$, $F = 434.7$, $R^2 = 0.94$; Fig. 22B); O₂ increased significantly from 0.29 mmol to 17.2 mmol ($P < 0.001$, $F\text{-stat} = 75.8$, $R^2 = 0.96$; Fig. 22C), and N₂ was estimated to increase significantly from 0.11 mmol to 16.2 mmol ($P < 0.001$, $F\text{-stat} = 277.5$, $R^2 = 0.91$; Fig. 22D).

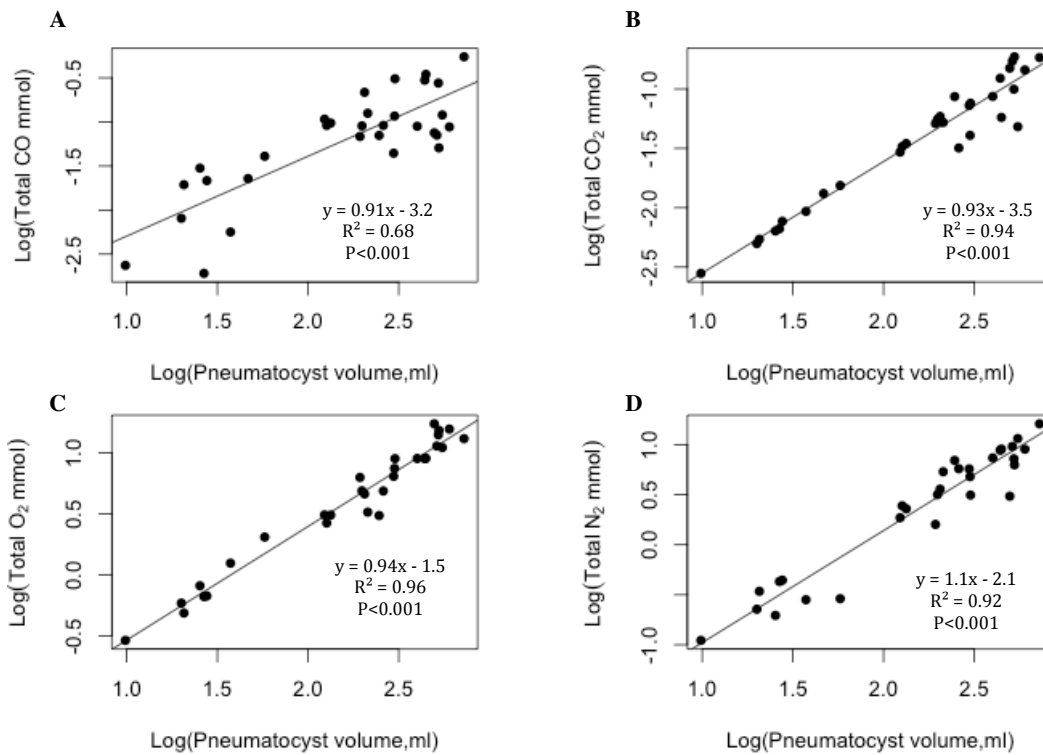


Figure 22: Log total gas for different pneumatocyst volumes (10-1000ml).

The concentration of CO in *Nereocystis* pneumatocysts was approximately 48,000 times greater than in air (Fig. 23; Table 3). The concentration of CO₂ in pneumatocysts was 15 times greater than in air (Fig. 23; Table 3). The concentration of O₂ was 2.8 times greater than in air (Fig. 23; Table 3). The concentration of N₂ was half as much as that in air (Fig. 23; Table 3).

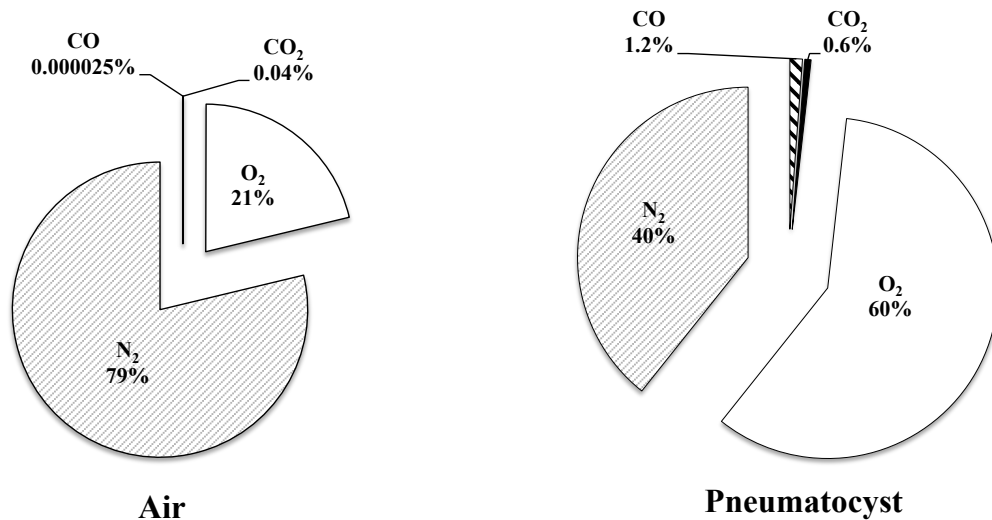


Figure 23: Average concentrations of gases in air compared to average concentrations of gases in a pneumatocyst. Pneumatocyst gas concentrations were compared to atmospheric gas concentrations by using information available online from the National Oceanic and Atmospheric Administration (NOAA.gov, USA).

Gas	Air	Pneumatocyst
CO	$2.5 \times 10^{-5}\%$	$1.2 \pm 0.78\%$
CO ₂	0.04%	$0.6 \pm 0.15\%$
O ₂	20.90%	$60 \pm 17.2\%$
N ₂	78%	$40 \pm 13.7\%$

Table 3: Table showing average gas concentrations of air and a pneumatocyst. Standard deviation of gas concentrations in a pneumatocyst is expressed in. Pneumatocyst gas concentrations were compared to atmospheric gas concentrations by using information available online from the National Oceanic and Atmospheric Administration (NOAA.gov, USA).

2.3.2 Pressure and CO₂ fluctuations

The SA:V decreases from 2.5 to 0.9 as pneumatocyst volume increases from 19 ml to 380 ml ($R^2 = 0.83$; Fig. 24A) By using the line fitted in Fig. 24A, pneumatocysts in the pressure experiment were estimated to have a SA:V between 1.2 and 2.4 as pneumatocysts increased in volume from 19 ml to 300 ml (Fig. 24B). The amplitude, or difference between the highest concentration of CO₂ and the lowest concentration of CO₂ (per sample) did not significantly change with increased pneumatocyst volume ($P > 0.05$; Fig. 24B). Throughout the experiment, CO₂ diurnally fluctuated 78.1 ± 13 ppm (Fig. 24B).

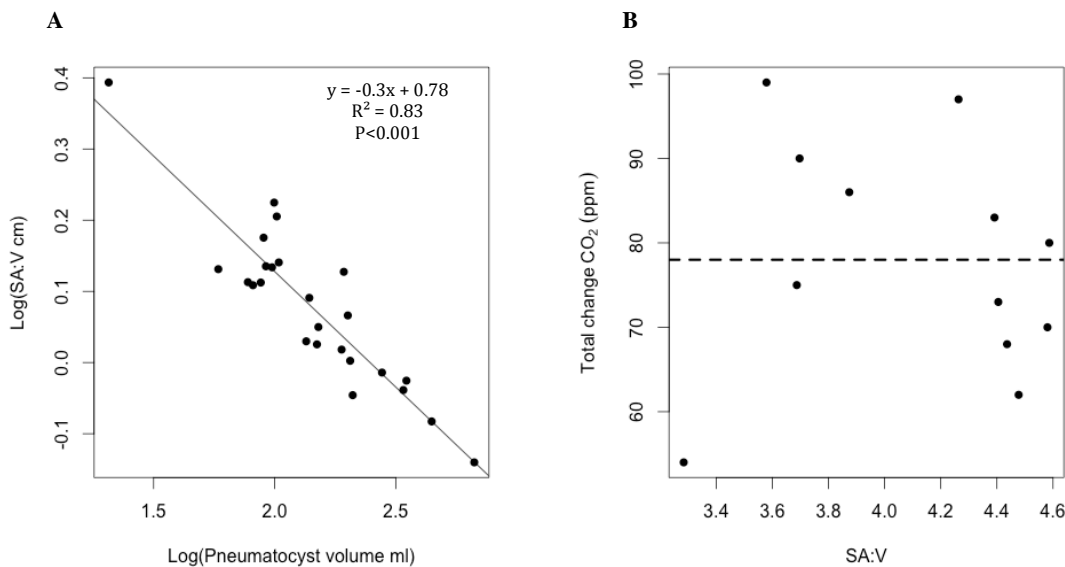


Figure 24: Log inner surface area to volume ratio (SA:V) for various pneumatocyst volumes (A). The total change or fluctuation of CO₂ for experimental pneumatocysts of various pneumatocyst volumes (B; $P > 0.05$). SA:V is estimated with the regression model in part A. Grey dotted line indicates the average fluctuation of CO₂.

Light intensity increased throughout the day from 0 to $500 \mu\text{mol m}^{-2} \text{s}^{-1}$ (Fig. 25A). Internal pneumatocyst pressure increased with increasing light exposure from 100.7 to 101.2 kPa (between 5:30 and 13:30) and then decreased from 101.2 to 100.8 kPa when light intensity decreased from $500 \mu\text{mol m}^{-2} \text{s}^{-1}$ to $0 \mu\text{mol m}^{-2} \text{s}^{-1}$ (between 13:30 and

21:30; Figs. 25A-B). Internal pneumatocyst pressure was lowest (100.4 kPa) at 1:30 when exposed to darkness for 4 hours (21:30 to 1:30; Figs. 25A-B). As internal pressure increased from 100.7 to 101.2 kPa, concentrations of CO₂ decreased from 75 ppm to 5 ppm (Figs. 25B-C). Concentrations of CO₂ were greatest at 5:30 (75 ppm) when the pneumatocyst was exposed to darkness from 21:30 to 5:30 (Fig. 25C).

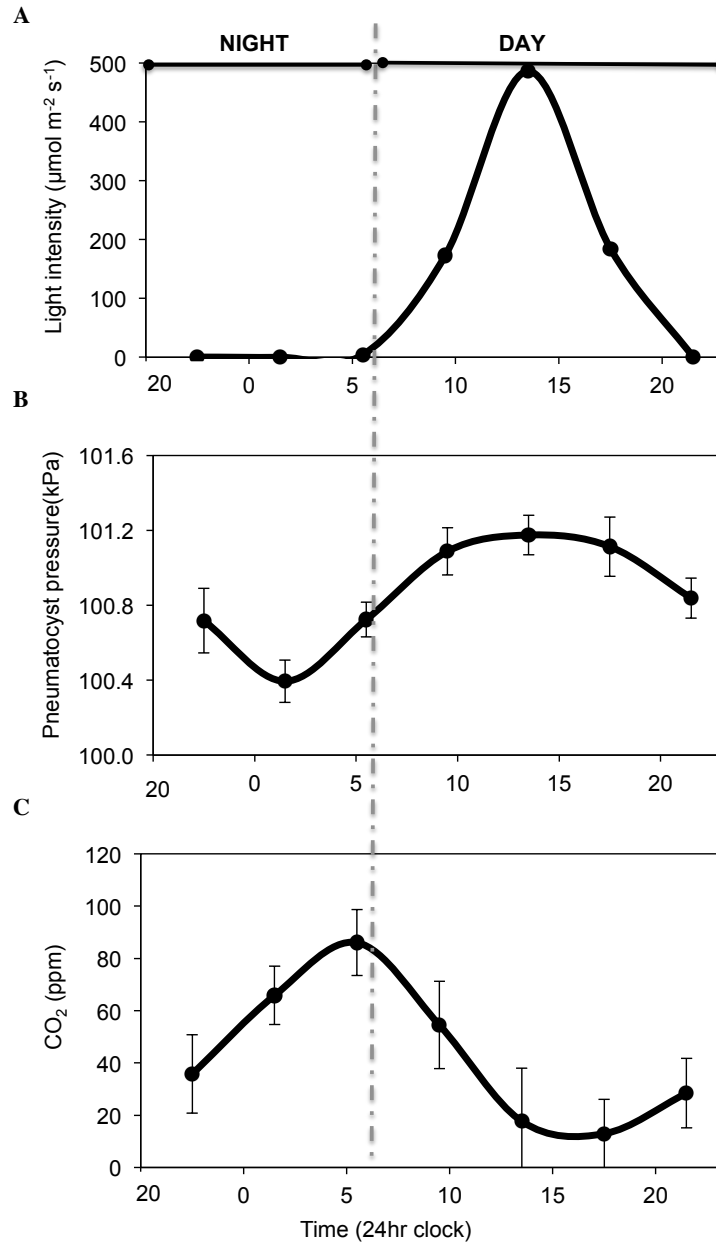


Figure 25: Changes of light (A), internal pneumatocyst pressure (B), and CO₂ concentration (C) during a 24 hour time period starting at 21:30. All data points represent average values. Error bars indicate standard deviation.

2.3.3 Pneumatocyst buoyancy

Thallus tissue density was $1090 \pm 0.1 \text{ kgm}^{-3}$. Thallus weight increased from 0.003 N to 1.65 N (0.01 to 3.01 kg) as thalli grew and pneumatocyst volume increased from 5 ml to 207 ml ($P < 0.001$, $F = 16.63$, $R^2 = 0.32$; Fig. 26A). Net buoyancy decreased from 2.21 N to 0.27 N with increasing thallus size ($P < 0.001$, $F = 20.8$, $R^2 = 0.38$; Fig. 26B). Therefore, total buoyant force did not change significantly with increasing thallus size ($P > 0.05$; Fig. 26C), averaging $1.36 \pm 0.5 \text{ N}$ at all size classes.

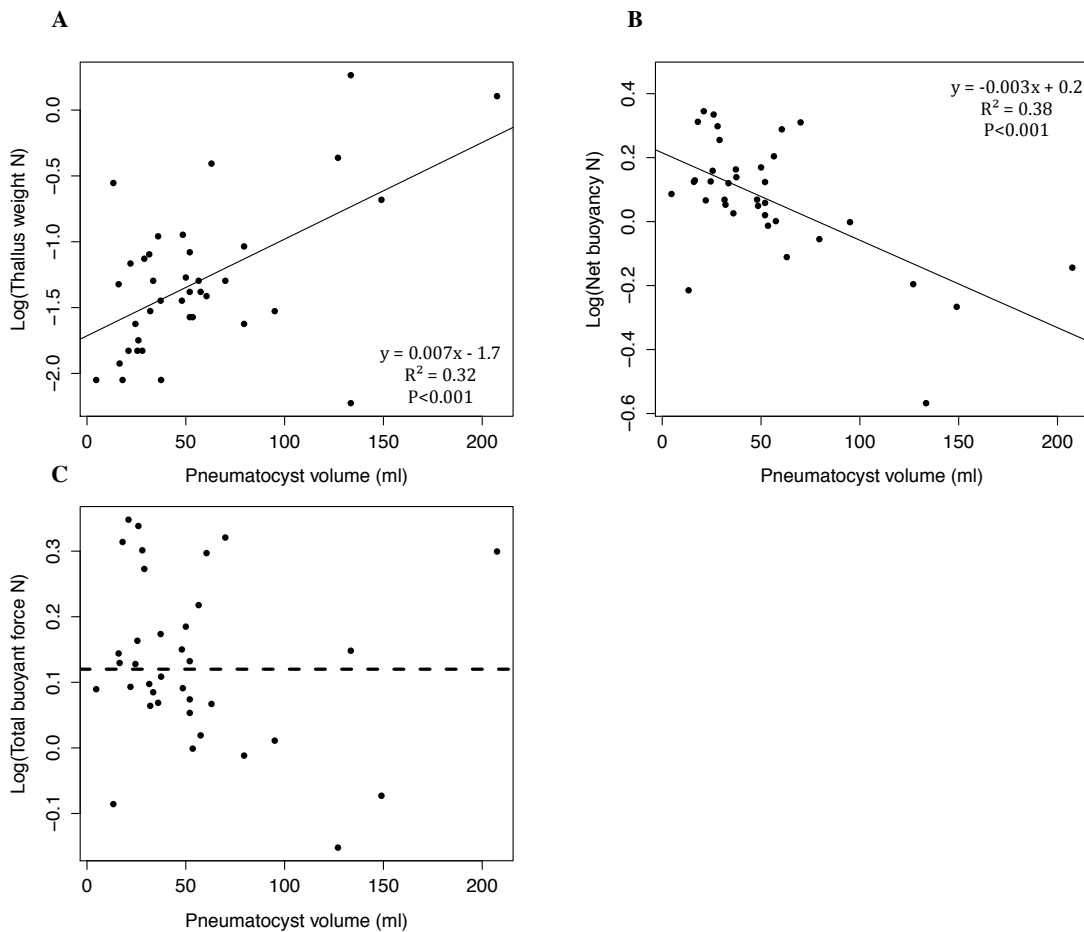


Figure 26: Log thallus weight (downward force, N) as a function of pneumatocyst volume (A). Log net buoyancy (upward force measured in Fig II.4, N) as a function of pneumatocyst volume (B). Log total buoyant force (upward force, N) as a function of pneumatocyst volume. Dotted line indicates average total buoyant force (C; $P > 0.05$).

Buoyant safety factor (BSF) was estimated to decrease from 432 to 1.6 with an increasing thallus size from 5 ml to 207 ml (Fig. 27). Average BSF of large individuals was 2.18 ± 1 (Table 4). Weighted down thalli had measured BSF values (grey data points) consistent with calculated BSF values ($P < 0.001$, $F = 22.56$, $R^2 = 0.41$; Fig. 27). According to the linear regression, growing thalli are estimated to sink when pneumatocyst volume exceeds 1.3 L (Fig. 27).

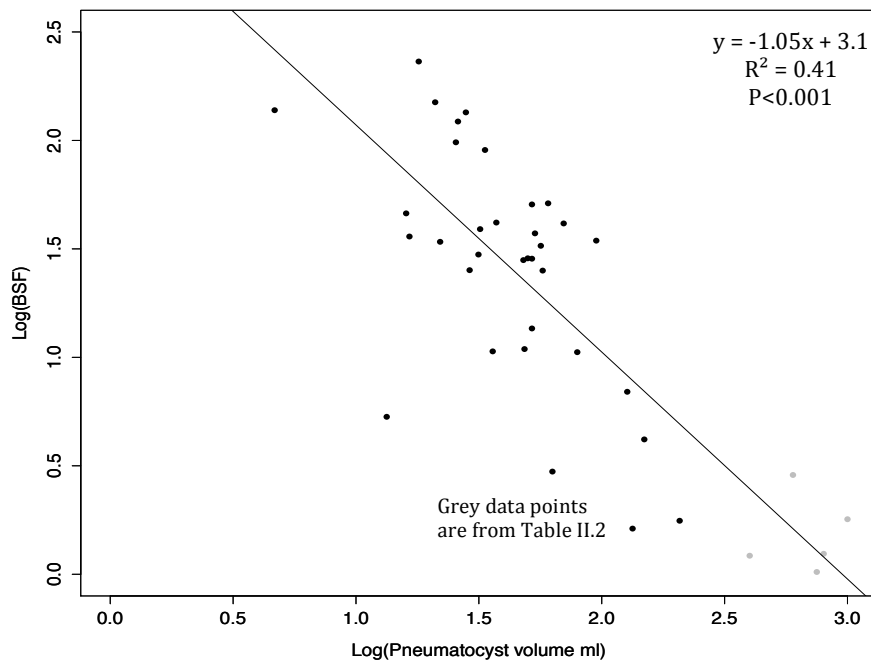


Figure 27: Log buoyant safety factor (BSF) as a function of Log pneumatocyst volume. The last 5 data points are represented in table II.2.

W_{th} (N)	$W_{th} + W_{added}$ (N)	BSF
1.02	1.83	1.79
1.75	2.18	1.25
0.15	0.68	4.53
0.67	1.06	1.58
0.34	0.64	1.88

Table 4: Table showing buoyant safety factor (BSF) calculated from 5 large pneumatocysts. Average BSF is 2.18 ± 1.3 .

2.4 Discussion

2.4.1 Pneumatocyst gas composition

Contrary to expectations, as pneumatocysts of *Nereocystis* develop and become larger in volume, overall gas composition does not change significantly (Fig. 21). The same relative proportions of gases are added/subtracted to pneumatocysts as they grow larger, and therefore the overall amount of gas increases with an increase in pneumatocyst volume (Fig. 22). Through in-situ lab trials, Foreman (1976) showed that the total amount of CO increases almost proportionally to increased wall thickness. This result could be extrapolated to all pneumatocyst gases since it is well known that the pneumatocyst wall becomes thicker with increased volume (Nicolson 1970) and regression lines fitted in Fig. 22 shows an almost proportional increase in mmol of CO, CO₂, O₂, and estimated N₂ per 1 ml of gas. This suggests that the rate of input and output of gases could be the same, and thus the same relative proportion of gases being added at all stages of development.

Pneumatocysts that are larger and have been increasing volume for a longer period of time have a greater amount of CO than younger, smaller pneumatocysts. A larger amount of CO present in older pneumatocysts suggests that CO is produced during all developmental stages. The most recent study examining the presence of CO in *Nereocystis* suggested that CO production is a product of cell degradation/tearing (autolysis) from the rapidly expanding pneumatocyst (Foreman 1976). Foreman (1976) argued his study provides evidence towards this hypothesis because the input of CO had slowed or subsided when the pneumatocyst stopped increasing volume (Foreman 1976), as stipe growth slowed near the water's surface (Duncan 1973). Therefore individuals

sampled once stipe growth has slowed could have lower CO concentrations than individuals undergoing stipe elongation (Foreman 1976). This study supports these findings since Fig. 22 depicts an increase in the total amount of CO (mmol) with increased size.

Earth's atmosphere contains only a small amount of CO (~0.000025%) whereas pneumatocysts contain an average concentration of 1.6% (Fig. 23). A study conducted by Langdon (1917) determined whether or not the concentration of CO was at a toxic level by exposing pneumatocyst gases to animals and measuring their physiological effects. Subsequently, the statement familiar to most phycologists, that the pneumatocysts of *Nereocystis* have enough CO "to kill a chicken" was a product of Langdon (1917). Without harming any animals, data collected during this study can further support this statement. 1.6% CO is a potentially toxic amount given that concentrations of CO greater than 100 ppm (0.01%) could kill or render a person unconscious (Suner et al. 2008). Given that an average adult male has a lung capacity of 5800 ml and the largest recorded pneumatocyst in this study (725 ml) had a CO concentration of 1.6%, if an average sized man inhaled the gas inside the largest sampled pneumatocyst, then in one breath he would ingest 1500 ppm of CO, 15-times greater than the maximum concentration a person could tolerate before passing out.

The CO₂ concentration in the pneumatocyst is generally about 0.6% (Fig. 21). The concentrations of CO₂ measured were similar to previous studies, which stated that about 0.5 to 1.7% of CO₂ was found in the pneumatocyst (Rigg and Swain 1941; Langdon and Galley 1920). Previous studies have found that pneumatocysts contain

approximately 21-25% O₂ (Langdon and Galley 1920; Rigg and Swain 1941). Contrary to earlier studies, this study found that there is an average of 60% O₂ in pneumatocysts (Table 3). Differences in the methodology of collecting and storing gas samples between this current study and Rigg and Swain (1941) could attribute to the discrepancies between the measured concentrations of O₂. Rigg and Swain (1941) extracted and stored pneumatocyst gas in wax sealed syringes prior to analyses, which may have been prone to leaking. The septum-sealed Exetainers used to store gases in this study have been shown to minimize air contamination and gas leakage up to 5 weeks after the sample is deposited (Glatzel and Well 2008). In this particular study, all gases were analyzed within 3 days of being extracted from the pneumatocyst. Therefore, I believe using the Exetainers used in this study could have yielded more accurate O₂ storage and measurements.

Estimated concentrations of N₂ in the pneumatocyst averaged about 40% (Table 3). These estimates were generally lower than previous studies which suggested that 78 to 80% of the pneumatocyst was comprised of N₂ and similar to the concentration in air (Langdon 1917; Langdon and Galley 1920). Though N₂ was only estimated in this particular study, higher measured concentrations of O₂ yielded these estimations to be less than previously measured concentrations. N₂ is an inert gas and does not play an integral role in cellular processes such as photosynthesis and respiration. If gas composition changed as a function of SA:V, larger pneumatocysts would have relative gas concentrations similar to air. These estimations for relative concentrations of N₂ further suggest that gas stored in the

pneumatocyst is not directly influenced by a decrease in SA:V as pneumatocysts grow larger.

2.4.2 Pressure and CO₂ fluctuations

Though Rigg and Swain (1941) demonstrated that internal pressure of adult pneumatocysts fluctuates as a response to changes in pneumatocyst gas composition, this study suggests that the magnitude of these fluctuations do not significantly change during pneumatocyst development. This experiment therefore demonstrates that internal pressure and CO₂ fluctuate similarly across all pneumatocyst sizes. Contrary to expectations, the decrease in surface area to volume ratio (SA:V) as pneumatocysts become larger does not influence pressure or gas fluctuations (Fig. 24). It is possible that cells in smaller pneumatocysts do not utilize the total pneumatocyst surface area to produce gases and cells in larger pneumatocysts over use their allocated surface area.

Calculations used to estimate SA:V generally represent the true SA:V of a pneumatocyst. Pneumatocysts have an odd geometry, making it difficult to accurately calculate surface area using generic equations formatted for specific geometric shapes, such as a sphere. Pneumatocysts change geometry as they increase volume. Generally, younger, smaller pneumatocysts are spherical until they reach a volume greater than 100 ml. At this point in development, the pneumatocyst extends into the stipe creating a hollowed cylinder to further hold gas and increase total volume. SA:V in the spherical apex of the pneumatocyst shown in Fig. 24A will increase by a factor of 3 divided by the sphere's inner radius. The changes in SA:V of the added cylinder is not much different since SA:V will increase by a factor of 2 divided by the cylinder's inner radius.

Furthermore, changes in SA:V are independent of cylinder height since radius is increasing at a rate much greater than the stipe being hollowed.

This in-situ experiment showed that internal pressure decreases at night, as the concentration of CO₂ increases accordingly, and internal pressure increases throughout the day, as the concentration of CO₂ declines (Fig. 25). These findings further support the claim made by Rigg and Swain (1941) that the concentration of CO₂ is less when it is utilized to produce O₂ via photosynthesis during the day, and the concentration of CO₂ is high when O₂ is utilized via cellular respiration during the night, leaving additional CO₂ as a byproduct. Thus, the levels of CO₂ measured in this experiment are reflecting the changes in O₂ diurnally due to photosynthesis and respiration. Furthermore, since this study also suggests that O₂ takes up more than half of the total gas present in the pneumatocyst, the utilization of O₂ during cellular respiration at night is more likely to influence the decrease in overall pressure of the pneumatocyst than CO₂ being added.

2.4.3 Pneumatocyst buoyancy

Surprisingly, the buoyant force from the pneumatocyst is eventually outpaced by the weight of growing thalli, and the risk of sinking increases. As individuals become larger with increased pneumatocyst volume, the overall weight of thalli also increases (Fig. 26). When the sporophytes grow and develop, their stipes begin to elongate, increasing light availability for their blades (Duncan 1976). This growth period inevitably results in heavier thalli with blades that can weigh up to 20 kg in air, creating a downward force that acts against the buoyant pneumatocyst (Denny et al. 1997). The total buoyant force does not significantly change with thallus size and pneumatocyst

volume (Fig. 26C), suggesting that increased pneumatocyst volume and buoyancy barely offsets the weight of the thalli. Although it is expected that a larger pneumatocyst volume would result in a larger buoyant force to offset the increased blade weight, the pneumatocyst material becomes thicker and the stipe becomes longer. Thus, as pneumatocysts increase in volume there is more thallus tissue, creating a greater mass that prevents the pneumatocyst from pushing upwards as much as might be expected. With increased thallus weight and no change in total buoyant force, the overall net buoyancy decreases as the pneumatocyst grows larger in volume (Fig. 26B).

Buoyant safety factor (BSF) decreases as thalli become heavier (Fig. 27). Alexander (1988) considered that the optimal safety factor for a biological structure could be estimated by analyzing the probability of failure (in this case, sinking), cost of structural maintenance, and the cost of structural failure. In the case of the pneumatocyst on *Nereocystis*, cost of structural failure is high in sporophytes since there is only one pneumatocyst and it cannot be regenerated. Without pneumatocysts, thalli could not remain upright, and would be left growing near the substrate, near hungry herbivores, and in low light, ultimately decreasing fitness (Chenelot and Konar 2007). During the early stages of *Nereocystis* sporophytes, pneumatocysts have a high BSF (Fig. 27). A high safety factor suggests that the probability of pneumatocysts sinking is low. In this case, there would also be an associated cost of maintenance in having a pneumatocyst buoyant force much greater than the weight it is trying to support.

On the contrary, the calculated BSF for older, reproductive sporophytes is low. To maintain buoyancy, the pneumatocyst would have to increase buoyant force as the thallus grows larger and becomes heavy. Taking into consideration the annual life history of

Nereocystis, the cost of failure in the pneumatocyst is low once the sporophyte has produced reproductive sori during late summer. *Nereocystis* stipes also have an environmental safety factor that decreases with age (Johnson and Koehl 1994). The cost of breakage is higher in younger thalli and lower in older thalli after sori production (Johnson and Koehl 1994). Both safety factors suggest a reduction in mechanical maintenance of large sporophytes since the thalli will most likely be dislodged and no longer viable during early winter storms.

The BSF is generally low for the five largest recorded thalli (Fig. 27; Table 4). Table 4 shows the calculated BSF values for these samples, revealing that all except one sample have a BSF less than 2. Pneumatocyst size is correlated with age and can be used as a proxy to roughly estimate total thallus size (weight) (Duncan 1973; Nicolson 1970). Therefore, the largest possible sporophyte that can remain upright (BSF=1) would have a pneumatocyst that is roughly 1.3 L (Fig. 27). If this sporophyte were to add any more blade weight, the 1.3 L pneumatocyst would no longer be able to keep the thallus upright, and the thallus would sink. The largest collected pneumatocyst in this study was roughly 1.2 liters (see Ch.1), just 100 ml less than the aforementioned estimate.

2.4.4 Conclusion

In conclusion, the relative proportions of CO, CO₂, O₂, and estimated N₂ gases do not significantly change as pneumatocysts grow and increase volume. Unlike what was found in previous studies, pneumatocyst concentrations of O₂, N₂, CO, and CO₂ were 59%, 40%, 1.6%, and 0.6% respectively. Furthermore, internal pneumatocyst pressure fluctuations do not change in magnitude, as pneumatocysts grow larger. These data

suggests that pneumatocyst SA:V does not influence the exchange in physiological gases over a diurnal light period.

As thalli grow larger, they also become heavier, causing the net buoyant force of pneumatocysts to decrease. Net buoyancy decreases because the total buoyant force of the pneumatocyst does not change as thalli become heavier. These results suggest that the total buoyant force is eventually outpaced by the weight of growing thalli, and the risk of the pneumatocyst sinking increases. Buoyant safety factor (BSF) decreases as thalli become heavier, suggesting that larger individuals are just buoyant enough to offset the thallus weight. Given trends in BSF, I predict that the largest possible sporophyte that could remain upright (BSF=1) would have a pneumatocyst that is roughly 1.3 liters, closely matching observed maximum size of *Nereocystis* in the field (1.2 L).

Conclusion

Maintaining buoyancy with pneumatocysts is essential for subtidal seaweeds with long flexible thalli, such as *Nereocystis luetkeana*, to achieve an upright stature and compete for light. However, as *Nereocystis* grows, pneumatocysts are exposed to significant changes in hydrostatic pressure. Exposure to changing hydrostatic pressure could cause complications since the pneumatocyst is filled with gases that may expand or contract, potentially causing pneumatocysts to break, flood, and no longer be buoyant. This study explored how *Nereocystis* pneumatocysts resist biomechanical stress and serves to keep the developing sporophyte upright in the water.

In Chapter 1, I demonstrated that pneumatocyst volume does not change passively with decreasing hydrostatic pressure, and increases by a factor of 400. Furthermore, pneumatocyst internal pressure does not passively change with hydrostatic pressure. These results indicate that pneumatocysts are not passive but rather actively regulated, and biological processes such as photosynthesis, respiration, and gas composition likely regulate internal pressures. Pneumatocysts are constantly exposed to a positive pressure gradient and experience compression. The difference in external hydrostatic pressure and internal pneumatocyst pressure becomes greater with depth and therefore smaller pneumatocysts experience the greatest loads. Pneumatocysts do not adjust geometry or material properties to reduce wall stress, which suggests that pneumatocysts are designed to tolerate compressive loads. Since the contribution of pneumatocyst geometry, material properties and the difference in force applied by internal and hydrostatic pressure does not reduce material stress, pneumatocysts found at depth are at greatest risk of buckling. Small pneumatocysts with inner radius of 0.8-0.9 cm and wall thickness of 0.2 cm were

found to be at a critical size, where the risk of buckling was greatest, since they are found at depth with high material stresses when compressive forces are greatest. These findings indicate that sporophytes reach a critical survival point early in their development, where success in growing to adulthood depends on the ability of small pneumatocysts to resist buckling.

Previous studies have suggested that light attenuation limits the maximum depth of sporophytes in the field to 35 m. However, considering spherical geometry and material properties, small pneumatocysts are also predicted to buckle at 35 m depth, close to the maximum depth observed in the field. Thus, the present study demonstrates that hydrostatic pressure, not just light attenuation, might attribute to the lower limit of *Nereocystis* in the field.

In Chapter 2, I explored changes in pneumatocyst gas composition and buoyancy through sporophyte development. This study demonstrated that the composition of gases in the pneumatocyst do not change as they develop and grow. The rate of input and output of gases is almost proportional to changes in pneumatocyst volume, suggesting that the same relative proportion of gases is being added at all stages of development.

Pneumatocyst gas composition is very different than the composition of atmospheric air, indicating that pneumatocysts are actively regulated, and biological processes such as photosynthesis and respiration likely contribute to the total gas composition found in pneumatocysts. Particularly, a pneumatocyst has enough CO to not only kill a chicken, but also an adult man. Contrary to previous studies, pneumatocyst concentrations of O₂, N₂, CO, and CO₂ were 59%, 40%, 1.6%, and 0.6% respectively. Furthermore, internal pneumatocyst pressure fluctuations do not change in magnitude, as

pneumatocysts grow larger, suggesting that pneumatocyst SA:V does not influence the exchange in physiological gases over a diurnal light period. Since O₂ takes up more than half of the total gas present in the pneumatocyst, the utilization of O₂ during cellular respiration is more likely to influence the decrease in overall pressure of the pneumatocyst than the increase in CO₂.

As total buoyant force is steadily outpaced by the weight of growing thalli, Adult pneumatocysts are ultimately at risk of sinking. There is a reduction in buoyancy maintenance of the pneumatocyst when sporophytes become massive in the fall, and they are dislodged during storms. Given the decrease in buoyant safety factor over time, the maximum size of adult sporophytes was predicted to be limited by a maximum pneumatocysts volume of 1.3 L, where any extra added weight (i.e. blades) would cause the thallus to sink. The largest collected pneumatocyst was roughly 1.2 liters, just 100 ml less than this prediction.

Given that buoyancy is essential for *Nereocystis*, data presented here may help to explain how pneumatocysts maintain buoyancy throughout development, highlighting the resilience of the pneumatocyst and its contribution to the growth and development of sporophytes.

Future directions

People have been studying kelp and pneumatocysts for over 100 years (MacMillan 1899; Sykes 1908; Zeller and Neikirk 1915; Frye 1915), yet there are still many questions about their biology. Specifically, research has been conducted on pneumatocysts investigated their gas composition and development (Rigg and Swain 1941; Langdon and Gailey 1920; Langdon 1917; Foreman 1976), but until this thesis, there has been little research on how internal pressure, gas composition, and biomechanical properties change as they grow and develop. Although this thesis discussed how the pneumatocyst of *Nereocystis* resists breaking under hydrostatic loads, there is little knowledge how other subtidal kelps cope with hydrostatic pressure (Ch.1). More specifically research has mainly focused on intertidal seaweeds with pneumatocysts tolerating fluctuations in hydrostatic pressure as the tide changes (Dromgoole 1981; Brackenbury et al 2006).

Although this study answered many questions regarding *Nereocystis* pneumatocysts, it also opened doors to more questions. In particular, not all material properties were tested due to time limitations and some values in estimating critical breaking depth need to be verified. Changes in material volume and Poisson's ratio should be measured to understand how the pneumatocyst material responds to compressive forces. Pneumatocysts were also collected no deeper than 10 m, and young pneumatocysts at 35 m depth should be collected for geometry, material properties, and material stress measurements. This will clarify if the calculated buckling wall stress is similar to what deeper pneumatocysts actually experience. Research in Chapter 2 suggested that the exchange of physiological gases in the pneumatocysts was not driven

by SA:V ratio. Results from this study suggested that the exchange of CO₂ in large pneumatocysts must be higher than predicted and might not be scaling with surface area. Therefore, further research is needed to understand how gas is exchanged in the pneumatocyst.

Macrocystis pyrifera (*Macrocystis*), develops pneumatocysts similar to that of *Nereocystis*, but instead of one pneumatocyst at the end of a single stipe, there are many pneumatocysts located along the length of each stipe, subtending each blade, and there are multiple stipes per individual. Unlike *Nereocystis*, pneumatocysts produced by *Macrocystis* stay at a fixed location throughout development along a given stipe. Therefore, these structures experience a constant hydrostatic load and this pressure differs depending on where the pneumatocyst develops along the stipe.

Future research should be conducted on how and if *Macrocystis* changes pneumatocyst material properties, geometry, and internal pressure to resist buckling under pressure. Like *Nereocystis*, *Macrocystis* pneumatocysts could have materials capable of tolerating high wall stresses. The spherical portion of the pneumatocyst of *Nereocystis* was at greatest risk of buckling. Unlike *Nereocystis*, *Macrocystis* creates pneumatocysts that are oblong, and possibly could have higher wall stresses, since hoop stress is 2 times greater in cylindrical objects compared to spherical objects. After showing that the net buoyancy of *Nereocystis* changes in accordance to its annual nature, I would expect that *Macrocystis* buoyancy does not significantly change annually. *Macrocystis* is not an annual, and has been recorded to have sporophytes that persist for up to 7 years, thus pneumatocyst buoyant force would need to increase as the thallus increases biomass and weight. Furthermore, instead of one stipe, *Macrocystis* has many,

which suggests that the loss of one stipe would have minimal consequences, to the survival of the sporophyte. Therefore, I predict that the BSF of *Macrocystis* would not change as the thallus increases size. It is likely that each pneumatocyst only needs to support the tissue between the pneumatocyst below it, and therefore any loss in tissue would not significantly change the sporophytes' buoyancy.

Another curious kelp, also closely related to *Nereocystis*, is *Pelagophycus porra* (*Pelagophycus*). *Pelagophycus* has a very similar morphology to *Nereocystis* except it is a deep-water species found between 25 m and 45 m. The pneumatocyst of *Pelagophycus* are capable of reaching a total volume similarly to *Nereocystis* at depth. As the pneumatocyst of *Nereocystis* increases in volume, the sporophyte increases stipe length, reducing hydrostatic pressure. Unlike *Nereocystis*, *Pelagophycus* develops a large pneumatocyst under hydrostatic loads that are much greater. Stipe elongation does not occur in *Pelagophycus* and thus the pneumatocyst develops while stationary at depth.

The internal pressure, material properties, and structural design of *Pelagophycus* pneumatocysts are under-studied. We know that *Nereocystis* pneumatocysts have an internal pressure that is less than atmospheric pressure since volume increases faster than the gas being added. *Pelagophycus* pneumatocyst growth rates and internal pressure are unknown. However, it is possible that growth is slower since the pneumatocysts are increasing volume under high hydrostatic loads. If this were the case, pneumatocysts would have an internal pressure less than hydrostatic pressure, but not nearly as low as the pressures measured in *Nereocystis*. Furthermore, unlike *Nereocystis*, the pneumatocyst of *Pelagophycus* would likely be at greatest risk of buckling when it is larger. A previous study suggested, that a large change in material modulus would be

needed to resist breaking as a pneumatocyst increases volume (Charters et al. 1969; Delf 1932). Therefore, the pneumatocyst would need to be stiffer with a high modulus, enabling the pneumatocyst to tolerate compressive loads.

References

- Abbott, I. A. & Hollenberg, G. J. 1976. *Marine Algae of California*. Stanford University Press, Stanford, CA, 827 pp.
- Alexander, R. MCN. 1988. The scope and aims of functional and ecological morphology. *Neth. J. Zool.* 38: 3–22.
- Arzee, T., Polne, M., Neushul, M. & Gibor, A. 1985. Morphogenetic aspects in Macrocytis development. *Botanical Gazette*: 365-374.
- Brackenbury, A. M., Kang, E.-J. & Garbary, D. J. 2006. Air pressure regulation in air bladders of *Ascophyllum nodosum* (Fucales, Phaeophyceae). *Algae* 21(2): 245-251.
- Brandt, P., Abson, D. J., DellaSala, D. A., Feller, R. & von Wehrden, H. 2014. Multifunctionality and biodiversity: Ecosystem services in temperate rainforests of the Pacific Northwest, USA. *Biological Conservation* 169: 362-371.
- Charters, A., Neushul, M. & Barilotti, C. 1969. The functional morphology of *Eisenia arborea*. In *Proc. Int. Seaweed Symp* 6: 89-105.
- Chenelot, H. and Konar, B., 2007. *Lacuna vincta* (Mollusca, Neotaenioglossa) herbivory on juvenile and adult *Nereocystis luetkeana* (Heterokontophyta, Laminariales). *Hydrobiologia* 583:107-118.
- Delf, E. M. 1932. Experiments with the stipes of *Fucus* and *Laminaria*. *Journal of experimental biology* 9(3): 300-313.
- Denny, M. & Cowen, B. 1997. Flow and flexibility. II. The roles of size and shape in determining wave forces on the bull kelp *Nereocystis luetkeana*. *Journal of experimental biology* 200(24): 3165-3183.
- Denny, M. W., Daniel, T. L. & Koehl, M. A. R. 1985. Mechanical limits to size in wave-swept organisms. *Ecological Monographs* 55(1): 69-102.
- Denny, M. W. 1988. *Biology and mechanics of the wave-swept environment*. Princeton University Press, Princeton, New Jersey, USA.
- Denny, M. W. & Hale, B. B. 2003. Cyberkelp: an integrative approach to the modeling of flexible organisms. *Philosophical Transactions of the Royal Society of London, Series B* 358: 1535-1542.
- Dromgoole, F. 1981. Form and function of the pneumatocysts of marine algae. I. Variations in the pressure and composition of internal gases. *Botanica Marina* 24(5): 257-266.

- Dromgoole, F. 1981. Form and function of the pneumatocysts of marine algae. II. Variations in morphology and resistance to hydrostatic pressure. *Botanica Marina* 24(6): 299-310.
- Duggins, D., Simenstad, C. & Estes, I. 1989. Magnification of secondary production by kelp. *Science* 24: 5.
- Duncan, M.J., 1973. In situ studies of growth and pigmentation of the phaeophycean *Nereocystis luetkeana*. *Helgoländer Wissenschaftliche Meeresuntersuchungen* 24(1-4): 510-525.
- Duncan, M. J. & Foreman, R. E., 1980. Phytochrome-mediated stipe elongation in the kelp *Nereocystis* (Phaeophyceae). *Journal of Phycology* 16(1): 138-142.
- Foreman, R.E. 1976., Physiological aspects of carbon monoxide production by the brown alga *Nereocystis luetkeana*. *Canadian Journal of Botany* 54(3-4): 352-360.
- Fournier, M., Stokes, A., Coutand, C., Fourcaud, T. and Moulia, B., 2006. Tree biomechanics and growth strategies in the context of forest functional ecology. *Ecology and biomechanics—a mechanical approach to the ecology of animals and plants* pp.1-33.
- Frye, T. 1915. *The Kelp Beds of South East Alaska*
- Frye, T. C., Rigg, G. & Crandall, W. 1915. The size of kelps on the Pacific Coast of North America. *Botanical Gazette*: 473-482.
- Gaylord, B., Blanchette, C. A. & Denny, M. W. 1994. Mechanical consequences of size in wave-swept algae. *Ecological Monographs* 64(3): 287-313.
- Gaylord, B. & Denny, M. W. 1997. Flow and flexibility I. Effects of size, shape and stiffness in determining wave forces on the stipitate kelps *Eisenia arborea* and *Pterygophora californica*. *Journal of experimental biology* 200: 3141-3164.
- Glatzel, S. & Well, R. 2008. Evaluation of septum-capped vials for storage of gas samples during air transport. *Environmental monitoring and assessment* 136(1-3): 307-311.
- Hein, M., Pedersen, M. F. & Sand-Jensen, K. 1995. Size-dependent nitrogen uptake in micro-and macroalgae. *Marine ecology progress series Oldendorf* 118(1): 247-253.
- Huston, R. and Josephs, H., 2008. *Practical stress analysis in engineering design*. CRC Press.
- Johnson, A. & Koehl, M. 1994. Maintenance of dynamic strain similarity and environmental stress factor in different flow habitats: thallus allometry and material properties of a giant kelp. *Journal of experimental biology* 195(1): 381-410.

Jung, C., Schindler, D., Albrecht, A. T. & Buchholz, A. 2016. The Role of Highly-Resolved Gust Speed in Simulations of Storm Damage in Forests at the Landscape Scale: A Case Study from Southwest Germany. *Atmosphere* 7(1): 7.

Kain, J. M. 1987. Patterns of relative growth in *Nereocystis luetkeana* (Pheophyta) 1. *Journal of Phycology* 23(1): 181-187.

Kármán, T.V and Tsien, H.S. 1941. The buckling of thin cylindrical shells under axial compression. *Journal of Aeronautical Sciences* 8: 303–312.

Koehl, M. A. R. & Wainwright, S. A., 1977. Mechanical adaptations of a giant kelp. *Limnology and Oceanography* 22(6): 1067-1071.

Langdon, S. C., 1917. Carbon monoxide, occurrence free in. 1(*Nereocystis luetkeana*). *Journal of the American Chemical Society* 39(1): 149-156.

Langdon, S. C. & Gailey, W. 1920. Carbon monoxide a respiration product of *Nereocystis luetkeana*. *Botanical Gazette*: 230-239.

Lubchenco, J. and Gaines, S.D., 1981. A unified approach to marine plant-herbivore interactions. I. Populations and communities. *Annual Review of Ecology and Systematics*, 12: 405-437.

MacMillan, C., 1899. Observations on *Nereocystis*. *Bulletin of the Torrey Botanical Club* 26(6): 273-296.

"National Oceanic And Atmospheric Administration". *Noaa.gov*. N.p., 2016. Web. 18 Mar. 2016.

Neushul, M. & Haxo, F. T., 1963. Studies on the giant kelp, *Macrocystis*. I. Growth of young plants. *American Journal of Botany*: 349-353.

Nicholson, N.L., 1970. Field studies on the giant kelp *Nereocystis* 1, 2. *Journal of Phycology* 6(2): 177-182.

Pan, B. & Cui, W., 2010. An overview of buckling and ultimate strength of spherical pressure hull under external pressure. *Marine Structures* 23(3): 227-240.

Pan, B., Cui, W., Shen, Y. & Liu, T. 2010. Further study on the ultimate strength analysis of spherical pressure hulls. *Marine Structures* 23(4): 444-461.

Rigg, G. B. & Swain, L. A. 1941. Pressure-composition relationships of the gas in the marine brown alga, *Nereocystis luetkeana*. *Plant physiology* 16(2): 361.

Rosenberg, G. & Ramus, J., 1984. Uptake of inorganic nitrogen and seaweed surface area: volume ratios. *Aquatic Botany* 19(1): 65-72.

Scagel, R. F., 1947. An Investigation on Marine Plants Near Hardy Bay. BC. *Provincial Department of fisheries*.

Sellier, D. and Fourcaud, T., 2009. Crown structure and wood properties: influence on tree sway and response to high winds. *American Journal of Botany*, 96(5), pp.885-896.

Sykes, M.G., 1908. Anatomy and histology of *Macrocystis pyrifera* and *Laminaria saccharina*. *Annals of Botany* 22(86): 291-325.

Spalding, H., Foster, M. S. & Heine, J. N., 2003. Composition distribution, and abundance of deep-water (>30m) macroalgae in central California 1. *Journal of Phycology* 39(2): 273-284.

Springer, Y., Hays, C., Carr, M. and Mackey, M.M., 2007. Ecology and management of the Bull Kelp, *Nereocystis luetkeana*. *Lenfest Ocean Program report*.

Stewart, H.L., Payri, C.E. and Koehl, M.A.R., 2007. The role of buoyancy in mitigating reduced light in macroalgal aggregations. *Journal of experimental marine biology and ecology* 343(1): 11-20.

Stewart, H. L., 2006. Ontogenetic changes in buoyancy, breaking strength, extensibility, and reproductive investment in a drifting macroalga *Turbinaria ornata* (Phaeophyta) *Journal of Phycology* 42(1): 43-50.

Stewart, H. L., 2006. Hydrodynamic consequences of flexural stiffness and buoyancy for seaweeds: a study using physical models. *Journal of experimental biology* 209(11): 2170-2181.

Sturm, K., Keller-Lehmann, B., Werner, U., Raj Sharma, K., Grinham, A. R. & Yuan, Z., 2015. Sampling considerations and assessment of Exetainer usage for measuring dissolved and gaseous methane and nitrous oxide in aquatic systems. *Limnology and Oceanography: Methods* 13(7): 375-390.

Suner, S., Partridge, R., Sucov, A., Valente, J., Chee, K., Hughes, A. & Jay, G. 2008. Non-invasive pulse CO-oximetry screening in the emergency department identifies occult carbon monoxide toxicity. *The Journal of emergency medicine* 34(4): 441-450.

Taylor, R. B., Peek, J. T. & Rees, T. A. V. 1998. Scaling of ammonium uptake by seaweeds to surface area: volume ratio: geographical variation and the role of uptake by passive diffusion. *Marine Ecology Progress Series* 169: 143-148.

Woodward, I., 2004. Plant science: tall storeys. *Nature* 428(6985): 807-808.

Zeller, S. M. & Neikirk, A. 1915. *Gas exchange in the pneumatocyst of Nereocystis luetkeana* (Mertens) P. & R. Puget Sound Marine Station.